WILEY
GLIA

RESEARCH ARTICLE OPEN ACCESS

Targeting Connexin 43 in Retinal Astrocytes Promotes Neuronal Survival in Glaucomatous Injury

Khulan Batsuuri[1] | Abduqodir H. Toychiev[1] | Suresh Viswanathan[2] | Stefanie G. Wohl[1] | Miduturu Srinivas[1]

[1]Department of Biological and Vision Sciences, SUNY College of Optometry, New York, New York, USA | [2]Indiana University School of Optometry, Bloomington, Indiana, USA

Correspondence: Miduturu Srinivas (msrinivas@sunyopt.edu)

Received: 23 August 2024 | **Revised:** 4 March 2025 | **Accepted:** 4 March 2025

Funding: This study was supported by National Eye Institute, EY028170 and RO1 EY032532.

Keywords: astrocytes | Connexin | gap junctions | glaucoma | hemichannels

ABSTRACT

Astrocytes in the retina and optic nerve head play an important role in the pathogenesis of glaucoma. Astrocytes extensively express connexin 43 (Cx43), a protein that forms gap junction (GJ) channels and transmembrane unopposed hemichannels. While it is well documented that Cx43 expression is augmented in retinal injuries, the role of astrocytic Cx43 channels in glaucomatous injury is not fully understood. Here, we used a mouse model of ocular hypertension caused by intracameral microbead injections and a more severe model, optic nerve crush (ONC) injury, and assessed changes in Cx43 expression and GJ channel function. The effect of astrocyte-specific deletion of Cx43 (Cx43KO) on retinal ganglion cell (RGC) loss and visual function was also assessed. We show that the Cx43 expression is increased in retinal astrocytes at early time points and remained elevated even after sustained elevation of intraocular pressure (IOP) (~8 weeks), which paralleled an increase in astrocytic GJ coupling. Deletion of astrocytic Cx43 markedly improved the survival of RGCs by ~93% and preserved visual function as assessed by ERG and reduced numbers of activated microglial/macrophages in the glaucomatous retina. Cx43 expression was also substantially increased after ONC injury, and the absence of Cx43 in this model increased RGC survival by ~48%. These results reveal a deleterious role for Cx43 in glaucoma progression. Intravitreal injections of Gap19, a peptide that reportedly inhibits Cx43 hemichannels but not GJ channels, markedly increased RGC survival and visual function. Further studies are required to assess whether targeting Cx43 hemichannels might be useful for glaucoma treatment.

1 | Introduction

Glaucoma is a neurodegenerative disease characterized by progressive and irreversible loss of retinal ganglion cells (RGCs) and their axons that lead to vision impairment (Foster et al. 2002; Miller and Quigley 1988; Quigley et al. 1981). Elevated intraocular pressure (IOP) is considered a major risk factor in glaucomatous injury, and consequently, the use of IOP-lowering drugs is a mainstay of therapy for glaucoma. However, a significant number of glaucoma patients continue to have progressive vision loss despite IOP-lowering treatments, emphasizing the need to identify alternate cellular mechanisms that contribute to the loss of RGCs and their axons.

A common feature of glaucoma is the reactivity of astrocytes in the retina and in the optic nerve head (ONH), a site of active tissue remodeling and axonal damage in glaucomatous injury. Astrocyte reactivity is characterized by increased expression of glial fibrillary acidic protein (GFAP), hypertrophy, invasion of axonal bundles, changes in the expression of extracellular matrix proteins, and release of cytokines. Depending on the injury type and time course of the insult, astroglial reactivity

appears to mediate both beneficial (Livne-Bar et al. 2017; Sun et al. 2017) and detrimental (Dvoriantchikova et al. 2009; Pekny and Pekna 2014; Pekny et al. 2014) effects on RGC function. Gene profiling studies of reactive astrocytes indicate that a subset of them adopts a neurotoxic phenotype in response to chronic IOP elevation and optic nerve crush (ONC) (Guttenplan et al. 2020).

Astrocytes abundantly express connexin 43 (Cx43), a protein that forms gap junctions (GJs) as well as unapposed hemichannels. GJs are formed when two connexin hemichannels dock together, leading to direct cell-to-cell communication, enabling transfer of metabolites and second messengers between adjacent astrocytes and other cells (Akopian et al. 2017, 2019; Slavi et al. 2018; Toychiev et al. 2021). In contrast, Cx43 hemichannels are mainly closed in physiological conditions (Contreras et al. 2003; Saez et al. 2005), but get activated in response to injury (e.g., hypoxia and ischemia) (Bennett et al. 2012; Calder et al. 2015; Contreras et al. 2002; Retamal et al. 2007). Their activation in such pathological conditions can cause the release of high levels of ATP and glutamate, leading to focal cytotoxicity via excessive purinergic or glutamatergic signaling (Bennett et al. 2012; Contreras et al. 2002; Danesh-Meyer et al. 2012; Davidson et al. 2013b; Froger et al. 2010; Kang et al. 2008; Orellana et al. 2011, 2012). Administration of Cx43 hemichannel inhibitors reduces astrogliosis (Ren et al. 2018) and neuronal damage in neurodegenerative diseases (Gajardo-Gomez et al. 2017; Wang et al. 2013; Yi et al. 2017).

It is well established that the expression of astrocytic Cx43 is increased in glaucomatous mice and in the retinal tissue of glaucoma patients (Danesh-Meyer et al. 2012; Kerr et al. 2011). The significance of this increased Cx43 expression, especially in long-term glaucomatous injury, is not fully understood. In addition, while the deletion of Cx43 in astrocytes does not affect glial or RGC function in the absence of injury (Slavi et al. 2018; Toychiev et al. 2021), the impact of Cx43-mediated intercellular communication and/or hemichannel opening on RGC loss in glaucoma remains largely unexplored. Here we studied the effect of astrocytic Cx43 deletion on RGC survival in murine models of chronic ocular hypertension and acute ONC injury, a more severe model to induce RGC death.

We demonstrate that the elevation of IOP increases Cx43 expression and augments GJ coupling in astrocytes. Astrocyte-specific deletion of Cx43 provides significant neuroprotection and preservation of visual function as assessed by electroretinogram (ERG) in glaucomatous mice. The absence of Cx43 in astrocytes also reduces microglial activation in glaucoma but does not affect astrocyte reactivity. Similarly, ONC injury increases Cx43 expression in the retina, and deletion of Cx43 significantly reduces RGC death. These results point to a vital contribution of astrocytic Cx43 to optic nerve damage. Finally, our results show that intravitreal injections of a peptide corresponding to the cytoplasmic loop of Cx43 (Gap19), which is reported to selectively inhibit hemichannels and not GJ channels, markedly improve RGC survival and function. These results suggest that targeting Cx43 hemichannels might be a new therapeutic approach to the treatment of glaucoma; however, additional studies are required to further test this hypothesis.

2 | Methods

2.1 | Animals

All mice were housed at the State University of New York, College of Optometry, Department of Biology and Vision Science. All mouse strains had a C57BL/6J background. Animals of both sexes were used. The transgenic mouse strains that were used in this study are:

1. *GFAP Cre*: $Cx43^{f/f}$: conditional knockout mice in which astrocytic Cx43 is deleted and are referred to as knockout (Cx43KO or KO) mice. mGFAP-Cre mice (Stock number 012886) were purchased from Jackson Laboratories.
2. $Cx43^{f/f}$: Cre negative Cx43 floxed (Stock number 008039, The Jackson Laboratory) mice were used as WT mice.
3. *GFAP Cre*: $stop^{f/f}$ *tdTomato*: Ai9 reporter mice (Stock number 007909, The Jackson Laboratory) (Madisen et al. 2010) which express tdTomato fluorescence in GFAP-expressing cells following Cre-mediated recombination;
4. $Cx43^{f/f}$: *GFAP Cre*: $stop^{f/f}$ *tdTomato*: Astrocyte-specific Cx43KO mice that express tdTomato fluorescence.

2.2 | Microbead Injections

The microbead occlusion model was used to achieve chronic elevation of IOP by injection of 10-μm-diameter polystyrene microbeads (Invitrogen) into the anterior chamber as previously described (Chen et al. 2011; Sappington et al. 2010). Mice were anesthetized with an intraperitoneal (i.p.) injection of a ketamine/xylazine mixture (70/7 mg/kg) and the cornea was punctured using a 30-gauge needle. The intracameral injections were performed unilaterally with 3 μL of microbead suspension using a Nanofil syringe (World precision instruments). An equivalent volume of sterile PBS was injected into the contralateral eyes to provide control (sham) measurements. A second microbead injection was performed in the fourth week, which maintained IOP at an elevated level for at least 4 more weeks. IOP was measured using a rebound tonometer (TonoLab; Colonial Medical Supply). Measurements were made within 1–3 min after the i.p. injection of the ketamine/xylazine mixture and topical application of 0.5% proparacaine. Subsequent weekly measurements were performed around the same time of day (± 30 min). Each weekly IOP measurement was averaged from five readings ($5 \times 6 = 30$) for each eye. Enucleations were performed at 4 and 8 weeks after the initial microbead injection, and retinas were isolated and assessed. In initial studies, we assessed whether contralateral eyes exhibited any changes compared to naïve eyes and found no significant difference between the two groups. Therefore, contralateral eyes were used as controls unless specified.

2.3 | Optic Nerve Crush Lesion

ONC lesion was inflicted by a previously described method (Isenmann 1997; Wohl 2011). Mice were anesthetized with an i.p. injection of a ketamine/xylazine mixture (70/7 mg/

kg). The optic bulb was protruded carefully, and the ON ~0.5–1 mm behind the eyeball was mechanically squeezed with fine, curved forceps for 5 s. ONC was done carefully not to disrupt the retinal blood supply. Animals were monitored on a heated pad for 2 h or until they recovered from anesthesia. Animals with signs of ischemia (hemorrhage, cloudy cornea, etc.) were excluded. Unoperated contralateral eyes were used as controls.

2.4 | Intravitreal Injection of Hemichannel Inhibitor Gap 19

Mice were anesthetized with an (i.p.) injection of a ketamine/xylazine mixture (70/7 mg/kg). After local anesthesia with proparacaine, the sclera was punctured with a 30-gauge needle, and 1 μL of Gap19 (200 μM final concentration) with a purity of 95% (Sigma-Aldrich), or TAT-Gap19 (200 μM final concentration) and TAT-Gap19 control scrambled peptide (200 μM final concentration) with purities of 95% (Tocris Bioscience) were intravitreally injected using a Hamilton syringe. All peptides were injected biweekly in one eye starting from the second week post microbead injection, while the other eye was injected with PBS. In a separate set of experiments, 1 μL of Gap 19 peptide (200 μM final concentration) (Sigma-Aldrich) was also injected in one eye every 2 weeks starting from the fourth week following post microbead injection.

2.5 | Immunohistochemistry

Whole eyeballs were enucleated and fixed in paraformaldehyde (PFA) solution (4% in PBS, Santa Cruz Biotechnology) for 20 min to 1 h at room temperature, followed by blocking with 3% (v/v) normal donkey serum (ThermoFisher) and 0.5% (v/v) Triton-X in PBS for 2 h at room temperature. Retinas were incubated with appropriate primary antibodies overnight at 4°C, washed with PBS, and further incubated with fluorescent secondary antibodies for 2 h at room temperature. The following primary antibodies were used: rabbit anti-Cx43 (Millipore Sigma, # C6219, 1:1000), goat anti-Brn3a (Santa-Cruz, # sc-31,984,1:500), mouse anti-Brn3a (Santa-Cruz, # sc-8429, 1:100) and guinea pig anti-RBPMS (PhosphoSolutions, # 1832, 1:500) for staining of RGCs; mouse anti-GFAP (Millipore Sigma, MAB 360, 1:1000) and rabbit anti-Sox9 (Sigma-Aldrich, # AB5535, 1:1000) for staining of astrocytes; goat anti-Iba1 (Abcam, # AB5076, 1:500) and rat anti-CD68 (Biolegend, # 137001, 1:500) for labeling of microglia (Table 1).

Primary antibodies were visualized using appropriate secondary antibodies (Table 2). Upon staining, whole retinae were mounted to glass slides using mounting medium with DAPI (Vectashield, Vector Labs).

2.6 | Confocal Microscopy and Quantitative Analysis

Images of immunolabeled tissues were taken using an Olympus FV1200MPE confocal microscope with 40× (oil immersion) objectives (Olympus, Tokyo, Japan). Four high-resolution (1024 × 1024 pixels) Z-stack images (317 × 317 μm) of RNFL and GCL (~15 μm) were taken from the midperipheral area in the wholemount retina using a step size of 1 μm, compiled into a single plane, and analyzed quantitatively. The cell counter function in ImageJ was used to measure astrocyte and ganglion cell numbers. Cx43 puncta number, size, and immune-positive area (% area) were analyzed with puncta analyzer (ImageJ plug-in), with the threshold for pixel size set from 1 to 20. Density analysis of astrocytes was performed to assess GFAP-positive immunolabeling using the particle analysis function in ImageJ. Images were converted to a black and white image with the threshold set above 4; this threshold value reduced interference from activated Müller cell end-feet from the density analysis of astrocyte reactivity in injury. The threshold parameters were identical for each measurement when comparing different groups. Quantification of GFAP-positive astrocyte reactivity was measured as the percentage of the area occupied by GFAP labeling in each region of interest.

2.7 | Quantitative Analysis of Microglia/Macrophages

We examined the changes in microglial morphology, cell density, and upregulation of the expression of the cell surface marker CD68, which are considered to be indicators of immune cell activation in glaucoma. Images of immunolabeled tissues

TABLE 1 | List of primary antibodies.

#	Primary antibody	Host	Company	Catalog#	Dilution
1	Cx43	Rabbit	Millipore Sigma	C6219	1:1000
2	Brn3a	Goat	Santa-Cruz	sc-31,984	1:500
3	Brn3a	Mouse	Santa-Cruz	sc-8429	1:100
4	RBPMS	Guinea pig	PhosphoSolutions	1832	1:500
5	GFAP	Mouse	Millipore Sigma	MAB360	1:1000
6	Sox9	Rabbit	Sigma-Aldrich	AB5535	1:1000
7	Iba1	Goat	Abcam	AB5076	1:500
8	CD68	Rat	Biolegend	137,001	1:500

TABLE 2 | List of secondary antibodies.

#	Secondary antibodies	Alexa Fluor	Company	Catalog #	Dilution
1	Donkey anti-goat	647	Thermofisher	A21447	1:500
2	Donkey anti-goat	594	Thermofisher	A11058	1:500
3	Donkey anti-rabbit	488	Thermofisher	A32790	1:500
4	Donkey anti-rabbit	647	Thermofisher	A32795	1:500
5	Donkey anti-rat	488	Thermofisher	A21208	1:500
6	Donkey anti-mouse	488	Thermofisher	A21202	1:500
7	Donkey anti-mouse	594	Thermofisher	A21203	1:500
8	Donkey anti-mouse	647	Thermofisher	A31571	1:500
9	Donkey anti-guinea pig	488	Millipore Sigma	SAB4600033	1:500
10	Donkey anti-rabbit	Texas Red	Santa-Cruz	sc-2784	1:500

were taken using an Olympus FV1200MPE confocal microscope with 40× (oil immersion) objectives (Olympus, Tokyo, Japan). Four high-resolution (1024×1024 pixels) Z-stack images (317 μm×317 μm) of the entire thickness of the retina were taken from the midperipheral area. Images were digitally dissected into GCL, OPL, and IPL and processed as described previously (Young and Morrison 2018). The following parameters were measured using ImageJ software (National Institutes of Health, Bethesda, MD, USA) to characterize microglial/macrophage activation: (1) endpoints per cell; (2) total branch lengths per cell. All cell numbers provided in the results are converted into per mm^2 area. At least four animals per group were analyzed.

2.8 | Dye Coupling/Neurobiotin Injection

Eyes were enucleated, and retinae were dissected in oxygenated HEPES buffer, transferred to filter papers (12-mm diameter cell culture inserts with 0.4-μm pore size, Sigma-Aldrich) and kept in a chamber constantly perfused with oxygenated bicarbonate extracellular buffer. A single astrocyte from each preparation was identified either based on the cell morphology and localization or based on its red fluorescence when GFAP tdTomato mice were used. The selected astrocyte was loaded with the GJ permeable tracer Neurobiotin (NB) (5 mg/ml) for 15 min. Immunohistochemistry was performed as described above. To ensure that the injected cells are astrocytes, retinae were stained with a mouse anti-GFAP primary antibody followed by a donkey anti-mouse secondary antibody conjugated with Alexa Fluor 647 (Thermofisher, # A21202, 1:500). Alexa Fluor 488-conjugated streptavidin (Thermofisher, # S32354, 1:500), which binds to NB, was used to visualize the NB-filled cells. Images of the entire thickness of retinas were taken using an Olympus FV1200MPE confocal microscope with 20× and 40× (oil immersion) objectives (Olympus, Tokyo, Japan). High resolution (1024×1024 pixels) Z-stack images of NB-labeled tissues were taken using a step size of 1 μm, compiled to a single plane of RNFL and INL, and converted to 3D reconstruction images by ImageJ. Astrocytes in RNFL and Müller cells in INL, labeled with NB, were counted manually in images obtained with confocal microscopy.

2.9 | Electroretinogram

ERGs were recorded from Cx43KO and WT mice 8 weeks after microbead-induced IOP elevation. Animals were dark adapted overnight and anesthetized with an i.p. injection of ketamine/xylazine (70/7 mg/kg) before recording under dim red light. Pupils were dilated with 2.5% phenylephrine hydrochloride/1% tropicamide, and the corneas were kept moist with 1% methylcellulose (Akorn). The body temperature was maintained around 37°C with an electric heating pad. ERGs were recorded with platinum electrodes placed in contact with the cornea, with needle electrodes inserted into the cheek and skin serving as reference and ground, respectively. Visual stimuli consisted of brief (< 5 ms) white full-field Ganzfeld flashes generated by an array of light-emitting diodes ranging from −6.7 to 2.0 log scot. cd.s/m^2 (Espion Color Dome stimulator; Diagnosys LLC, Lowell MA). Responses were averaged over 40–50 trials for weak stimuli and fewer trials for stronger stimuli. Signals were amplified, filtered (1–300 Hz) and digitized at 1 kHz with a resolution of 0.1 μV. The STR reflects the activity of RGCs (Saszik et al. 2002). The STR was elicited in the intensity range of −4.9 to −4.0 log scot. cd.s/m^2 and the amplitude of the positive STR (pSTR) was computed from the peak of the pSTR to the trough of the negative STR (nSTR). The b-wave amplitudes were measured at their peak from the b-wave trough. ERG data were extracted and analyzed using Sigma Plot software. Nine animals per glaucomatous group (WT and Cx43KO) and four naive controls were used.

2.10 | Quantitative PCR

The retinas were harvested and lysed with Trizol (Life Technologies, #15596026) (1 retina/500 μL of Trizol). Total RNA was extracted from whole retinas from WT and Cx43KO mice using the Direct-Zol RNA MiniPrep Plus kit (Zymo research). RNA samples were double treated with DNAse I (Zymo research) in the column and ezDNase (ThermoFisher) RT-PCR. Complementary DNA (cDNA) was synthesized using the SuperScript IV VILO Master Mix Kit (Invitrogen). qPCR was performed on a 96-well plate in the QuantStudio 7 Flex Real-Time PCR System (ThermoFisher). Primers were

TABLE 3 | Genes corresponding to A1, A2, and pan-reactive astrocytes and associated primers.

Markers		Gene	Forward	Reverse
A1	1	H2-T23	GGACCGCGAATGACATAGC	GCACCTCAGGGTGACTTCAT
	2	Serping1	ACAGCCCCCTCTGAATTCTT	GGATGCTCTCCAAGTTGCTC
	3	Fbln5	CTTCAGATGCAAGCAACAA	AGGCAGTGTCAGAGGCCTTA
	4	Amigo2	GAGGCGACCATAATGTCGTT	GCATCCAACAGTCCGATTCT
A2	1	S100a10	CCTCTGGCTGTGGACAAAAT	CTGCTCACAAGAAGCAGTGG
Pan-reactive	1	GFAP	AGAAAGGTTGAATCGCTGGA	CGGCGATAGTCGTTAGCTTC

obtained from Integrated DNA Technologies and shown in Table 3. Thermocycling conditions were 50°C × 2 min and 95°C × 2 min, followed by 40 cycles of 95°C for 15 s and 60°C for 1 min. Reactions were run in triplicates or duplicates for RT or –RT samples. Values were normalized to the housekeeping gene GAPDH. Delta delta Ct between Cx43KO and WT mice was calculated and expressed together with standard deviation (S.D). Three to seven animals per group (WT and Cx43KO) were used for each condition (naïve, 4 and 8 weeks after IOP elevation).

2.11 | Statistical Analysis

Two-sided two-sample Student's t test (H0: M1 = M2, H1: M1 ≠ M2) at the significance level of $\alpha = 0.05$ (95% confidence interval) was used for comparisons between mice groups of different genotypes (ex. WT versus Cx43KO mice). Two-sided one-sample Student's paired t test (H0: M = 0, H1: M ≠ 0) at the significance level of $\alpha = 0.05$ (95% confidence interval) was used for comparisons between retinae that received different injections (ex. SHAM versus microbead). One-way ANOVA at the significance level of $\alpha = 0.05$ (95% confidence interval), followed by Tukey's test, was used for comparisons between three or more time points. Two-way ANOVA at the significance level of a = 0.05 (95% confidence interval), followed by Tukey's test, was used for comparisons between the groups at different light intensities in ERG analysis. Statistical analyses were performed using the GraphPad Prism 8 software. Results are presented as mean ± SEM and n values correspond to the number of mice.

3 | Results

3.1 | Microbead-Induced IOP Elevation in WT and Cx43KO Mice

To induce experimental glaucoma, we adopted and implemented a microbead occlusion model of elevating IOP that involved the injection of 10-μm polystyrene microbeads into the anterior chamber of mouse eyes. As shown in Figure 1, intracameral injection of microbeads resulted in a significant elevation of IOP within 1 week. IOP showed a gradual decrease after 3 weeks, necessitating a second injection at 4 weeks, which enabled the IOP to be maintained at an elevated level for at least 8 weeks (Figure 1B). In WT mice ($n = 58$), the average IOP for the duration of 8 weeks was 14.0 ± 0.17 mmHg in control eyes, whereas microbead injection increased IOP by 32% (18.49 + 0.3, $p < 0.0001$). Microbead injections into the eyes of Cx43KO mice ($n = 50$) produced an equivalent level of IOP elevation as in WT, with no statistical difference in the peak IOP between the two groups ($p = 0.87$). Sham injections of PBS did not markedly increase the IOP in WT or Cx43KO animals (Figure 1C).

3.2 | Sustained Elevation of IOP Induces RGC Death

RGC loss was assessed following 2, 4, and 8 weeks of elevated IOP in whole mount retinas with Brna3a, a marker that selectively labels ~85%–90% of RGCs (Figure 1D). RGC counts were obtained from the midperipheral region from four retinal quadrants of identical size (~1.5–2.0 mm from the optic disk) of glaucomatous retina and were compared to RGCs of contralateral and naïve eyes in WT mice. RGC counts from the contralateral eye were comparable to naïve eyes with no significant difference. Microbead-induced elevation of IOP did not induce significant RGC death 2 weeks after the initial injection (microbead-injected retina 3980 ± 273 versus control retina 4522 ± 62, $n = 3$, $p = 0.18$; data not shown). However, as shown in Figure 1E, there was significant RGC loss in glaucomatous retinas after 4 weeks (3504 ± 107.3, $n = 8$, $p < 0.0001$) of IOP elevation compared to control retinas (4618 ± 144.5, $n = 8$). Longer duration (8 weeks) of elevated IOP further exacerbated RGC degeneration (3157 ± 123.3, $n = 10$, $p < 0.0001$; decrease of 35%) compared to control (Figure 1E).

3.3 | Cx43 Expression Is Enhanced in Response to Glaucomatous Injury

Contralateral and bead-injected retina of WT mice were immunostained with anti-Cx43 (Figure 2A,B). There was a significant increase in Cx43 immunolabeling in astrocytes after sustained IOP elevation, with the number of Cx43 puncta increasing in the retina at 4 weeks and at 8 weeks after IOP elevation compared to contralateral controls ($n = 3$–5, $p < 0.05$) (Figure 2C). In addition, the average size of plaques corresponding to Cx43 increased by 16% and 24% at 4 weeks ($n = 3$, $p < 0.05$) and at 8 weeks ($n = 5$, $p < 0.05$), respectively, after initial microbead injection (Figure 2D). Together with increased size and counts, the overall percent area of Cx43 increased by 36% at 4 weeks ($n = 3$,

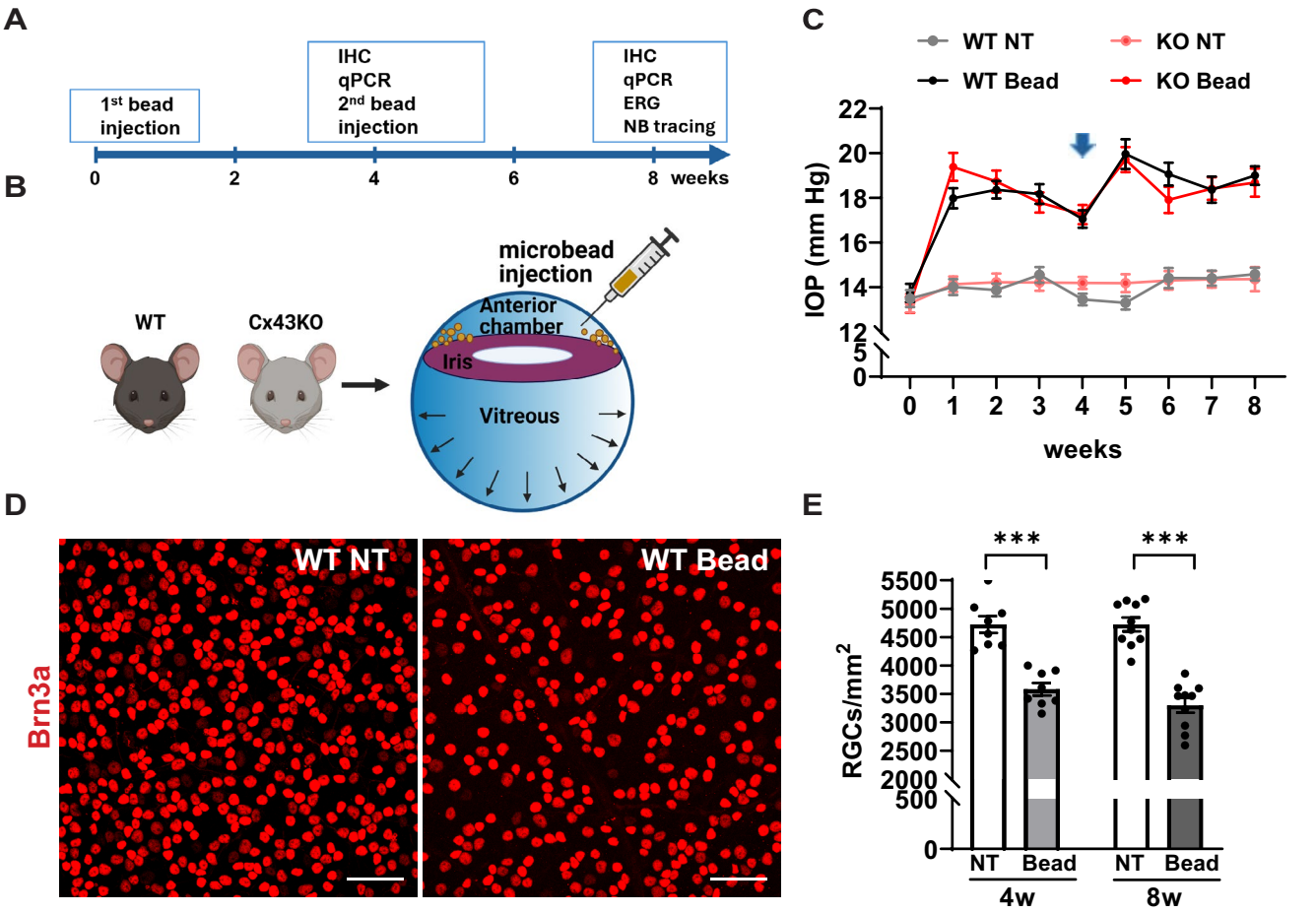

FIGURE 1 | Microbead occlusion model of glaucoma induces RGC loss. (A) Time points of experimental analysis. (B) Illustration of intracameral injection of polystyrene microbeads into WT and Cx43KO mice. (C) Data show sustained elevation of IOP ($p < 0.001$) in WT ($n = 58$) and KO ($n = 50$) compared to PBS-injected control eyes for 8 weeks after initial microbead injections at day 0. The second injection was administered 4 weeks after the first injection (arrow). There is no significant difference in IOP elevation between WT and KO mice ($p = 0.87$, Student's t test). (D) Immunofluorescent images of Brn3a positive RGCs in wholemount retinas of control (left; non-treated; NT) and bead-injected retinas (right) of WT mice at 8 weeks after microbead injection. (E) Quantification of Brn3a positive cells in control ($n = 18$) and 4 ($n = 8$) and 8 ($n = 10$) weeks after glaucomatous injury. ***$p < 0.001$, Student's t test. Scale bar 50 μm.

$p < 0.05$) and 75% at 8 weeks ($n = 5$, $p < 0.01$) (Figure 2E). Our result is in line with the previous studies that have reported an increased Cx43 expression in glaucomatous eyes of human patients (Kerr et al. 2011).

3.4 | Glaucomatous Injury Increases GJ Coupling Between Retinal Glial Cells in the Retina

We next assessed whether upregulation of Cx43 expression in glaucomatous retina correlates with an increase in astrocytic–astrocytic coupling (Figure 3A–C). IOP elevation was induced in reporter mice expressing tdTomato in astrocytes (by crossing a tdTomato reporter mouse with a mouse expressing Cre recombinase in GFAP locus) to visualize astrocytes, and individual astrocytes were loaded with Neurobiotin (NB) using whole-cell patch clamp. After 15 min of loading, the retinas were fixed and stained with fluorescent conjugated streptavidin to determine the extent of diffusion of NB dye to adjacent astrocytes through GJs. As shown in Figure 3D, chronic elevation of IOP for 8 weeks increased the number of NB labeled astrocytes (107 ± 15.72; $n = 7$, $p < 0.01$) compared to uninjured controls (55.71 ± 5.94; $n = 4$), indicating an increase in GJ coupling, consistent with the increase in Cx43 labeling in astrocytes. In contrast, NB labeling was restricted to a loaded astrocyte in Cx43KO retina as expected (see Figure 3C for a representative image).

Previous studies in rat and rabbit retina showed that astrocytes are directly coupled to Müller cells, the main glial cells in the retina (Robinson et al. 1993; Zahs and Newman 1997). To determine whether astrocytes are coupled to Müller cells in the mouse retina, we loaded NB for 15 min into individual tdTomato-expressing astrocytes in retinal whole mounts using whole-cell patch clamp. The retinas were then fixed and labeled with streptavidin conjugated to Alexa 488. Consistent with the previous data (Robinson et al. 1993; Zahs and Newman 1997), NB labeling was observed in the mouse INL where Müller cells somata reside (Figure 4A). Three-dimensional reconstructions of optical sections show Müller glia labeled in their entirety (Figure 4B). NB loaded into an individual astrocyte diffused to multiple Müller glia (around

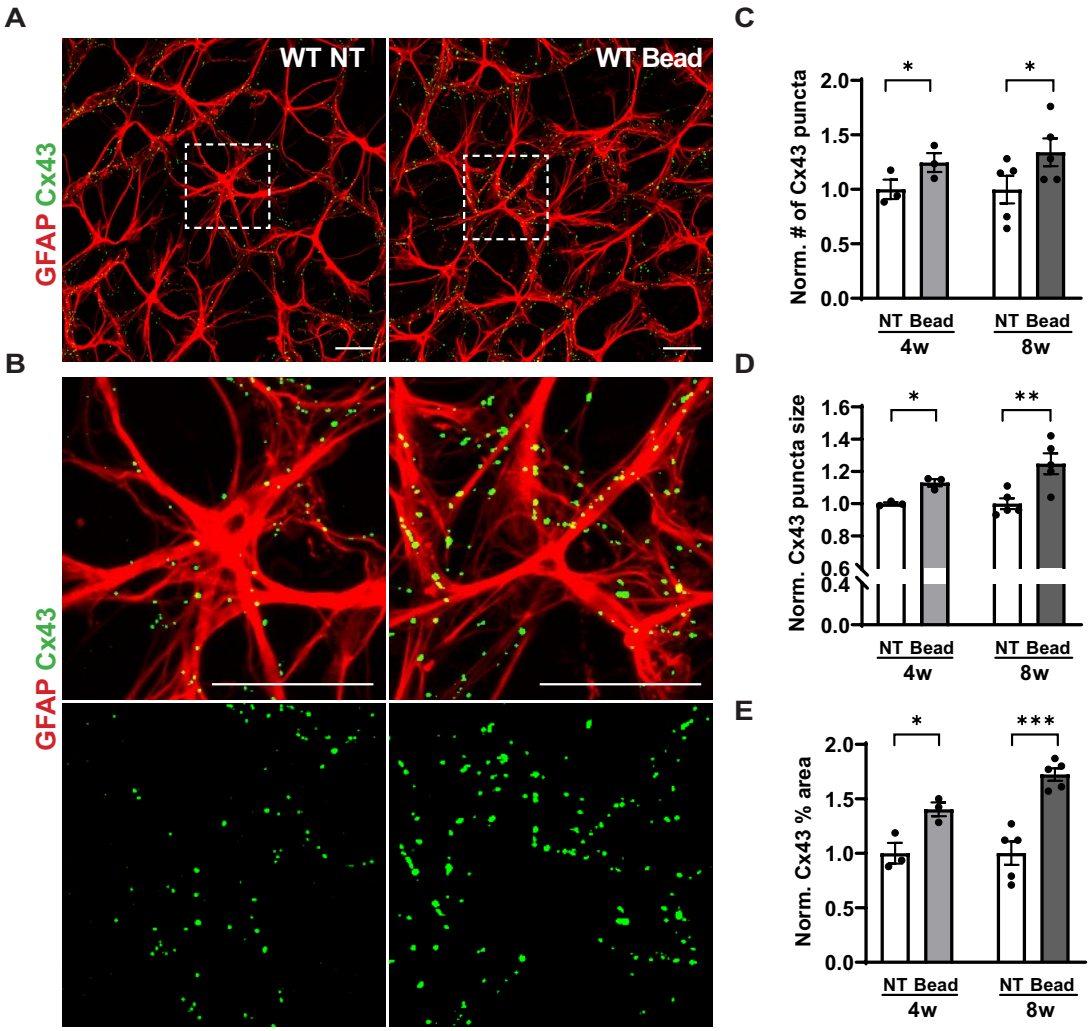

FIGURE 2 | Cx43 expression is increased in glaucomatous retina. (A) Representative images depict the Cx43 (green) expression in GFAP-positive astrocytes (red) in naive control (non-treated; NT) and glaucomatous retina in WT mice. (B) Panels are magnified images from the insets (white box), with panel A showing Cx43 puncta in astrocytes (top) and puncta alone (bottom) in control and injured retina. Quantification of Cx43 puncta per area (C) and normalized puncta size (D) percent area (E) show that the Cx43 expression is increased in the retina following sustained elevation of IOP ($n = 5$) compared with control ($n = 5$). Analysis of normalized Cx43 puncta size (D) demonstrates that Cx43 plaques are increased in size in glaucomatous retina ($n = 5$) compared with control ($n = 5$). *$p < 0.05$, **$p < 0.01$, ***$p < 0.001$, Student's t test. Scale bar 25 μm.

125 cells on average) in the uninjured retina. Interestingly, the majority of these coupled Müller cells did not express GFAP (Figure 4A). We next determined whether sustained IOP elevation also augments astrocyte-Müller glia connectivity (Figure 4A–D). Measurement of NB^+ Müller cells after 8 weeks of increased IOP revealed that the number of NB^+ Müller glia is increased by 3.8-fold in glaucomatous retina ($n = 5$, $p < 0.05$) (Figure 4D). Müller cells themselves remained uncoupled to each other after sustained IOP elevation (Figure 4C), suggesting that the increase in astrocyte-Müller cell coupling seen after chronic elevation of IOP is due to the increase of GJ connectivity between astrocytes. It is also possible that coupling between astrocytes and Müller cells is increased in response to IOP elevation. The connexins that are expressed in Müller cells at these hetero-cellular junctions are unknown, and we could not assess whether there is an increase in connexin expression in these glial cells.

3.5 | Deletion of Cx43 in Astrocytes Attenuates RGC Loss and Improves Retinal Function After Chronic Elevation of IOP

To determine the role of Cx43 in glaucomatous injury, we increased IOP in WT and Cx43KO mice and evaluated RGC survival using IHC. Retinal whole mounts were labeled with Brn3a 4 and 8 weeks after IOP elevation (Figure 5). Brn3a labeling in retinas of microbead-injected eyes was compared to both contralateral and naïve eyes in WT (see Figure 1D) and in Cx43KO mice (Figure 5A). There was significant cell loss (~25%) following 4 weeks ($n = 8$, $p < 0.0001$) of IOP elevation compared to controls ($n = 18$) (Figure 5B). Longer duration (8 weeks) of IOP increase further exacerbated RGC degeneration by up to ~35% ($n = 10$, $p < 0.0001$) compared to controls (Figure 5B). In comparison, deletion of Cx43 prevented RGC loss at both time points. Quantification of $Brn3a^+$ RGCs shows that astrocyte-specific

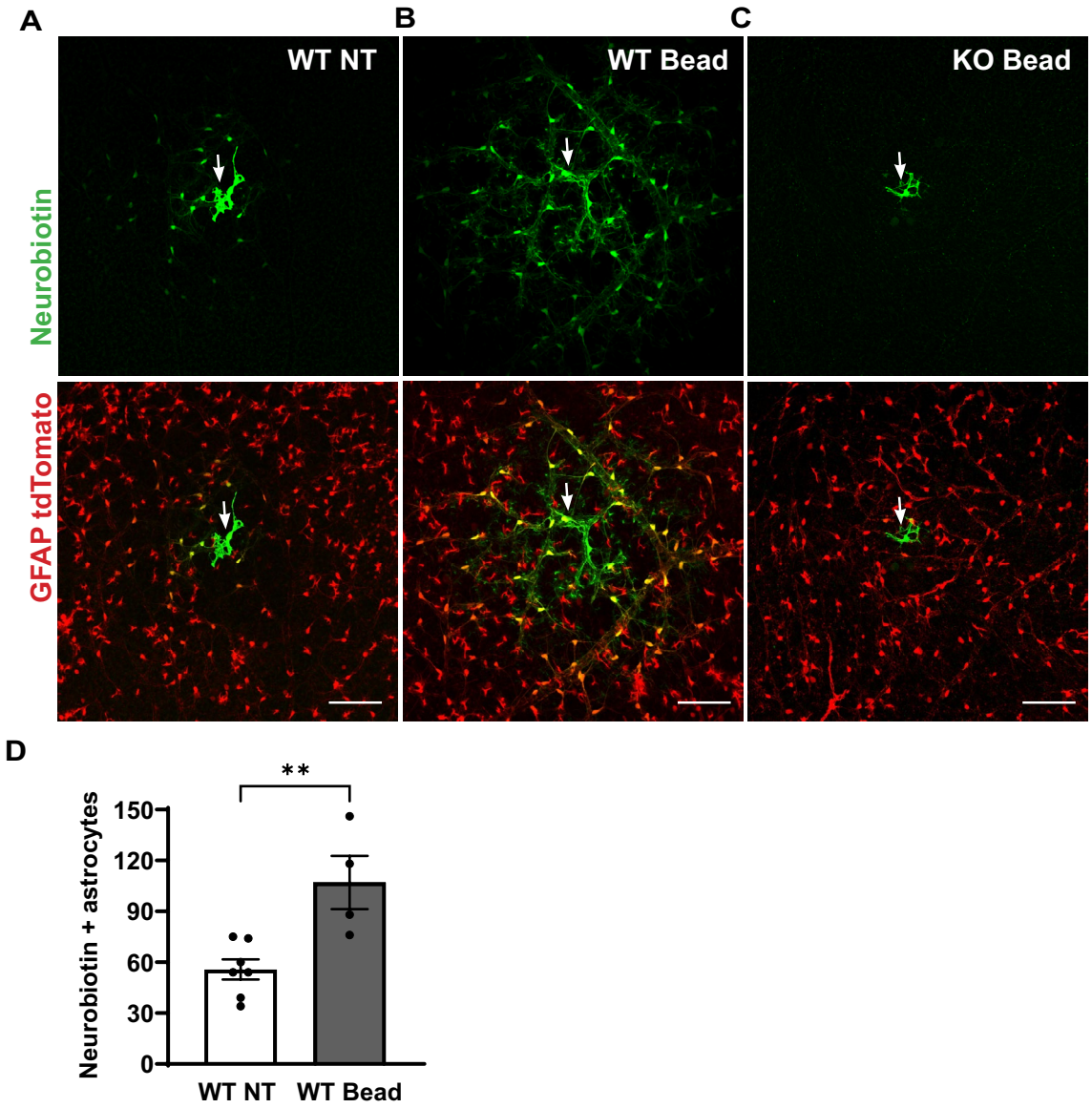

FIGURE 3 | Astrocytic coupling is increased in glaucoma. Representative images of neurobiotin (NB)-injected astrocytes in tdTomato-expressing control (A, non-treated (NT)) and 8 weeks after elevated IOP in WT (B) and Cx43KO (C) mice. NB labeling was restricted to the injected astrocyte in Cx43KO mice. (D) Quantification of NB positive astrocytes shows increase in astrocytic coupling in bead-injected WT retina ($n = 4$) compared to control ($n = 7$). $^{**}p < 0.01$, Student's t test. Scale bar 100 μm. Arrow: Injected astrocyte cell body.

deletion of Cx43 is neuroprotective, with RGC survival increasing by ~90%–93% after 4- ($n = 5$–8, $p < 0.001$) and 8-week ($n = 10$, $p < 0.0001$) IOP elevation compared to WT bead-injected eyes (Figure 5B).

To determine whether the absence of Cx43 astrocytes also preserves RGC function, we evaluated visual activity of WT and Cx43KO mice by recording dark-adapted ERG. Representative recordings of the pSTRs, a measure of RGC function, from WT and Cx43KO are shown in Figure 6A. The average pSTR amplitude was significantly reduced in WT mice by ~40%–50% (e.g., at −4.3 log.cd.s/m^2; $n = 9$, $p < 0.001$) after 8 weeks of IOP elevation, but this decrease was not observed in Cx43KO mice ($n = 9$, $p < 0.001$) (Figure 6B), indicating that the absence of Cx43 improved visual function, consistent with neuroprotection. Furthermore, elevation of IOP in WT resulted in a significant reduction in b-wave amplitude ($n = 9$, $p < 0.001$) indicating changes in bipolar cell activity, as previously reported (Bayer et al. 2001; Harazny et al. 2009; Kumar et al. 2021; Wang and Dong 2016). Deletion of Cx43 in astrocytes attenuated the decrease in b-wave amplitude ($n = 9$, $p < 0.05$), suggesting that the absence of astrocytic Cx43 prevents damage to the outer retina (Figure 6C).

3.6 | Deletion of Cx43 Does Not Affect Astrocytic Reactivity in Glaucomatous Retina

Increased GFAP expression is considered to be one of the main characteristics of reactive gliosis (Escartin et al. 2021; Sofroniew and Vinters 2010; Sun and Jakobs 2012; Sun et al. 2017; Tehrani et al. 2016, 2014). Therefore, we analyzed GFAP labeling density of astrocytes in the retina of IOP-elevated WT mice (Figure 7) and found moderate changes in GFAP expression, as evidenced by hypertrophy of astrocytic processes at 4 or 8 weeks.

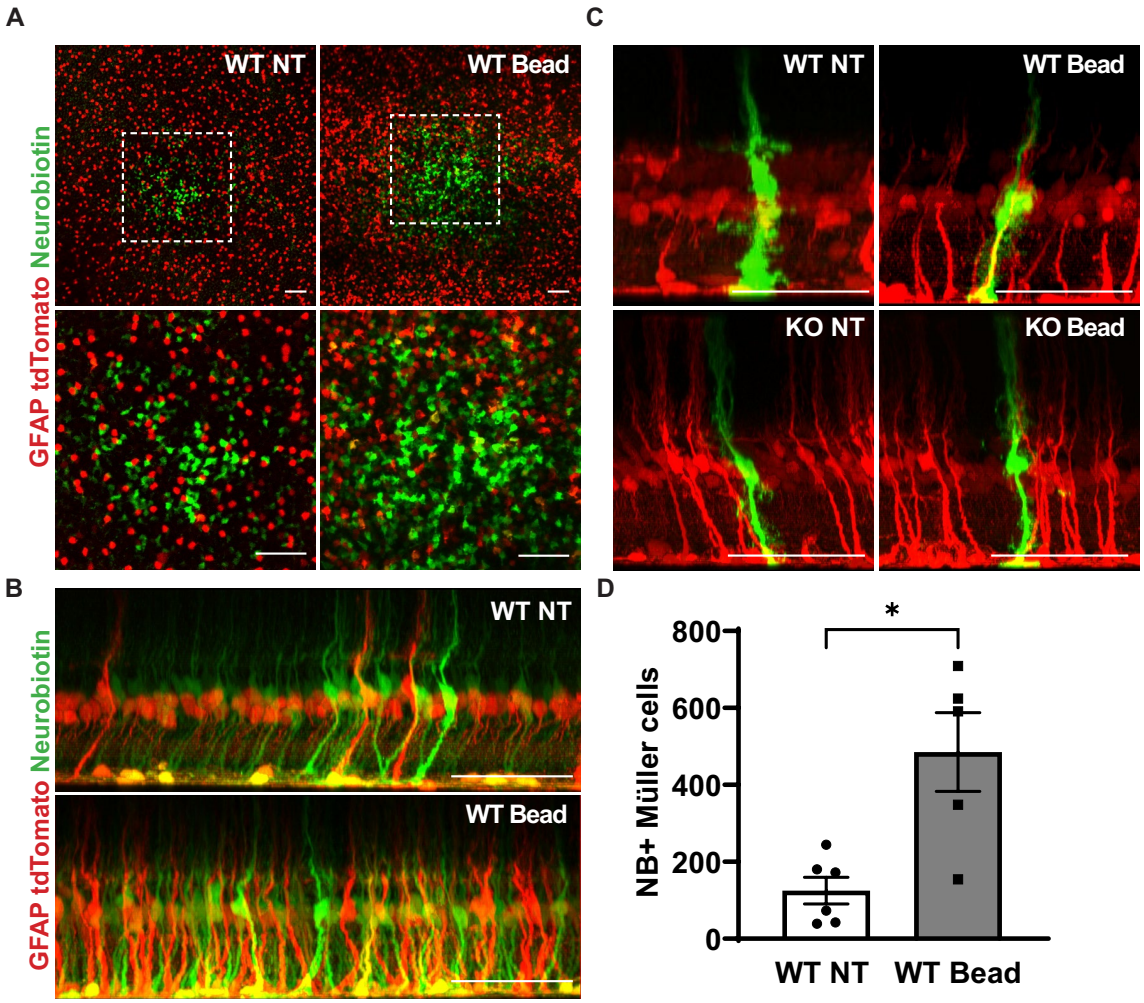

FIGURE 4 | Glaucomatous injury increases astrocyte-Müller cell coupling. (A) Representative images of neurobiotin (NB) positive Müller cells (green) in the INL of the retina in control mice and in mice exposed to 8 weeks of elevated IOP. NB was injected into a single astrocyte in the nerve fiber layer (not shown) of WT mice expressing tdTomato under a GFAP promoter (red). (B) 3D projection of whole mount retina in WT control (top) and bead-injected mice (bottom), showing that NB loaded to an astrocyte diffuses into Müller glia. (C) NB injected into a single Müller cell did not transfer to adjacent Müller cells in control or glaucomatous retinas of WT and KO mice. (D) Quantification of NB positive Müller glia. The number of Müller glia coupled to astrocytes is increased in bead-injected WT retina ($n = 5$) compared to control ($n = 6$). *$p < 0.05$, Student's t test. Scale bar 50 μm.

GFAP-positive area increased by 18%–20% at 4 or 8 weeks ($n = 6$, $p < 0.01$) of IOP elevation compared to the contralateral retina ($n = 6$). Importantly, this moderate increase of GFAP expression in the retina was not affected by deletion of Cx43 after 4 weeks ($n = 5$, $p < 0.01$) or 8 weeks ($n = 4$, $p < 0.05$) of IOP increase (Figure 7C).

Gene profiling studies indicate that a subset of reactive astrocytes adopts a neurotoxic phenotype in response to chronic IOP elevation and ONC (Guttenplan et al. 2020; Liddelow et al. 2017). This transcriptionally defined subset of astroglial cells, called A1 astrocytes, was induced in response to factors secreted by activated microglia (IL1a, TNFα and C1q) (Liddelow et al. 2017). Inhibiting the formation of neurotoxic astrocytes markedly increased RGC survival in glaucomatous injury (Guttenplan et al. 2020; Liddelow et al. 2017; Sterling et al. 2020). We hypothesized that Cx43 hemichannels and GJ channels may propagate signaling molecules associated with A1 neurotoxic astrocytes and exacerbate disease progression. Therefore, gene transcripts of reactive astrocytes in both naive and glaucomatous WT and Cx43KO mice were compared. We chose specific genes from pan-reactive, A1, and A2 neuroprotective astrocytes that showed the highest increases after nerve crush and IOP elevation from previous studies (Guttenplan et al. 2020; Liddelow et al. 2017). However, we did not see significant changes in the selected subset of A1 or A2 reactive transcripts at 4 or 8 weeks of IOP elevation. Relative mRNA levels of pan-reactive (GFAP), neurotoxic (Fbln5, Amigo2, H2-T23, Serping1) and neuroprotective astrocytes (S100a10) did not show specific changes in naïve Cx43KO mice ($n = 7$, $p > 0.05$) (Figure S1A) or in mouse cohorts in which there was sustained elevation of IOP ($n = 3$, $p > 0.05$) (Figure 7D). For example, we measured gene transcripts of reactive astrocytes in WT and Cx43KO mice 4 weeks after IOP elevation, a time point where reactive astrocyte transcripts are increased by ~20-fold on average (Guttenplan et al. 2020). Surprisingly, our data did not show such large increases in the expression of transcripts associated with A1 reactive astrocytes (Figure 7D), a difference likely due to technical and methodological differences. We performed conventional RT-PCR on whole retinal tissue

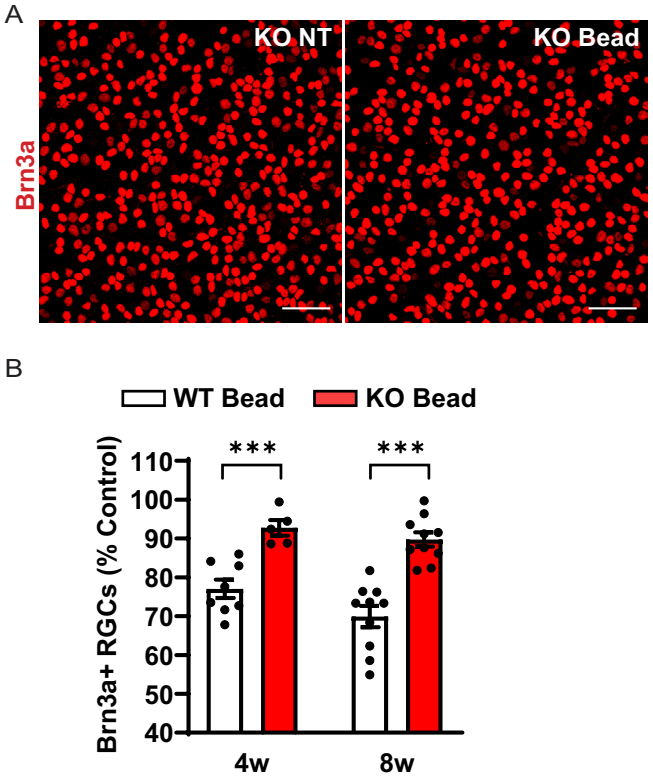

FIGURE 5 | Deletion of Cx43 increases RGC survival in glaucoma. (A) Representative images of control (left; non-treated (NT)) and bead-injected retina (right) of Cx43KO mice 8 weeks after elevated IOP. (B) Deletion of Cx43 in astrocytes increased RGC survival up to ~93% ($n=10$) at 4 weeks and ~90% ($n=7$, 8) at 8 weeks after elevated IOP. ***$p<0.001$, Student's t test. Scale bar 50 μm.

compared to microfluidic RT-PCR (Guttenplan et al. 2020), which might have dampened the effects that occur specifically in astrocytes. We also did not test gene expression in the ONH, where astrocytes are the dominant resident cells. Another limitation is that we chose a limited number of genes to test for the presence of A1 neurotoxic astrocytes. Broader selection of gene transcripts might provide a more detailed picture of A1 and A2 astrocyte profiling. However, our results are consistent with a recent study in ONH astrocytes that showed that A1 neurotoxic gene expression of reactive astrocytes was upregulated only at the early time points (7 or 14 days after bead injection) but returned to baseline by 4 weeks after elevated IOP (Tan et al. 2022), the time point employed in this study.

3.7 | Absence of Cx43 Reduces Microglial Reactivity in Glaucomatous Injury

Microglial activation has been reported to occur early in glaucomatous injury and contribute to RGC loss (Bosco et al. 2011; Kumar et al. 2023). In the normal retina, resting microglia have small cell bodies and highly ramified long processes and provide homeostasis. In response to injury, resting microglia become reactive and exhibit changes in morphology, acquiring an ameboid shape, expression of cell surface proteins like CD68 (Holness and Simmons 1993; Rice et al. 2017), MHCII (Chidlow et al. 2016; Kumar et al. 2023; Rojas et al. 2014) and production of pro-inflammatory cytokines (Giulian et al. 1986; Hanisch 2002; Nakazawa et al. 2006; Schroeter et al. 1997). To evaluate microglial activation, we labeled microglia with cell surface markers, Iba1 (Rojas et al. 2014) and CD68, in whole mount retina of WT and Cx43KO mice 8 weeks after IOP elevation (Figure 8). However, since blood-derived monocytes/macrophages express these markers and can infiltrate the retina after ocular hypertension (Huang et al. 2007; Margeta et al. 2018) we do not rule out the presence of macrophages in our study. Density and morphological analysis of microglia/macrophages were performed in the GCL, IPL, and OPL (Figure 8). The number of endpoints and average length of branches per cell were measured to assess morphological changes as previously described (Young and Morrison 2018).

Eight weeks after microbead injection, the density of Iba1+ microglia increased by 55% ($n=5$–9, $p=0.004$) in the GCL of WT mice compared to naive controls (Figure 8B). Similarly, the number of Iba1+ cells significantly increased in the IPL ($n=5$–9, $p=0.004$) (Figure 8C) and OPL ($n=5$–9, $p<0.0001$) (Figure 8D). Deletion of Cx43 in astrocytes resulted in significantly reduced microgliosis in the IPL ($n=5$, $p=0.01$) and OPL ($n=5$, $p<0.05$) and in the GCL ($n=5$, $p=0.13$); the decrease in the GCL, however, did not reach statistical significance. Overall, the total number of microglia/macrophages in the whole retina (GCL+IPL+OPL) is increased by 43% in glaucomatous WT mice ($n=5$, $p<0.0001$). Deletion of Cx43 alleviated the increase in microglia/macrophages numbers ($n=5$, $p<0.001$) (Figure 8E).

We also found fewer activated microglia in Cx43KO compared to WT mice after IOP elevation (Figure 9). We counted the numbers of Iba1+ cells that also express CD68, a cell surface marker of phagocytic microglia/macrophages. There were lower numbers of Iba1+/CD68+ cells in the whole retina (GCL+IPL+OPL) of bead-injected Cx43KO mice compared to WT mice (WT Bead: 343.3±14 vs. Cx43KO Bead: 269.2±20.6 cells/mm^2, $n=3$, $p<0.05$) (Figure 9E). Deletion of Cx43 in astrocytes reduced Iba1+/CD68+ cells specifically in the IPL (WT Bead: 136.7±5.8 vs. Cx43KO Bead: 103±9.5 cells/mm^2, $n=3$, $p<0.05$) and OPL (WT Bead: 160±1.6 vs. Cx43KO Bead: 139.2±5.8 cells/mm^2, $n=3$, $p<0.05$) after glaucomatous injury (Figure 9C,D). In response to prolonged elevation of IOP, microglia/macrophage morphology is dramatically altered, leading to the development of hypertrophic cell bodies with shorter and less ramified branches in bead-injected WT mice ($n=5$, $p<0.05$) compared to naïve control mice (Figure S2). However, the retraction of microglial branches was unaffected by the deletion of Cx43 (Figure S2).

3.8 | Cx43 Deletion Is Also Neuroprotective in the Optic Nerve Crush Model

Microbead injection model of glaucoma recapitulates the IOP-induced increase in progressive but moderate cell death. ONC is a more severe model for glaucoma as it induces significant RGC death that recapitulates certain characteristics of glaucomatous optic neuropathy. To study whether astrocytic Cx43 deletion is neuroprotective in acute form of neurodegeneration, we assessed Cx43 expression 7 days after ONC

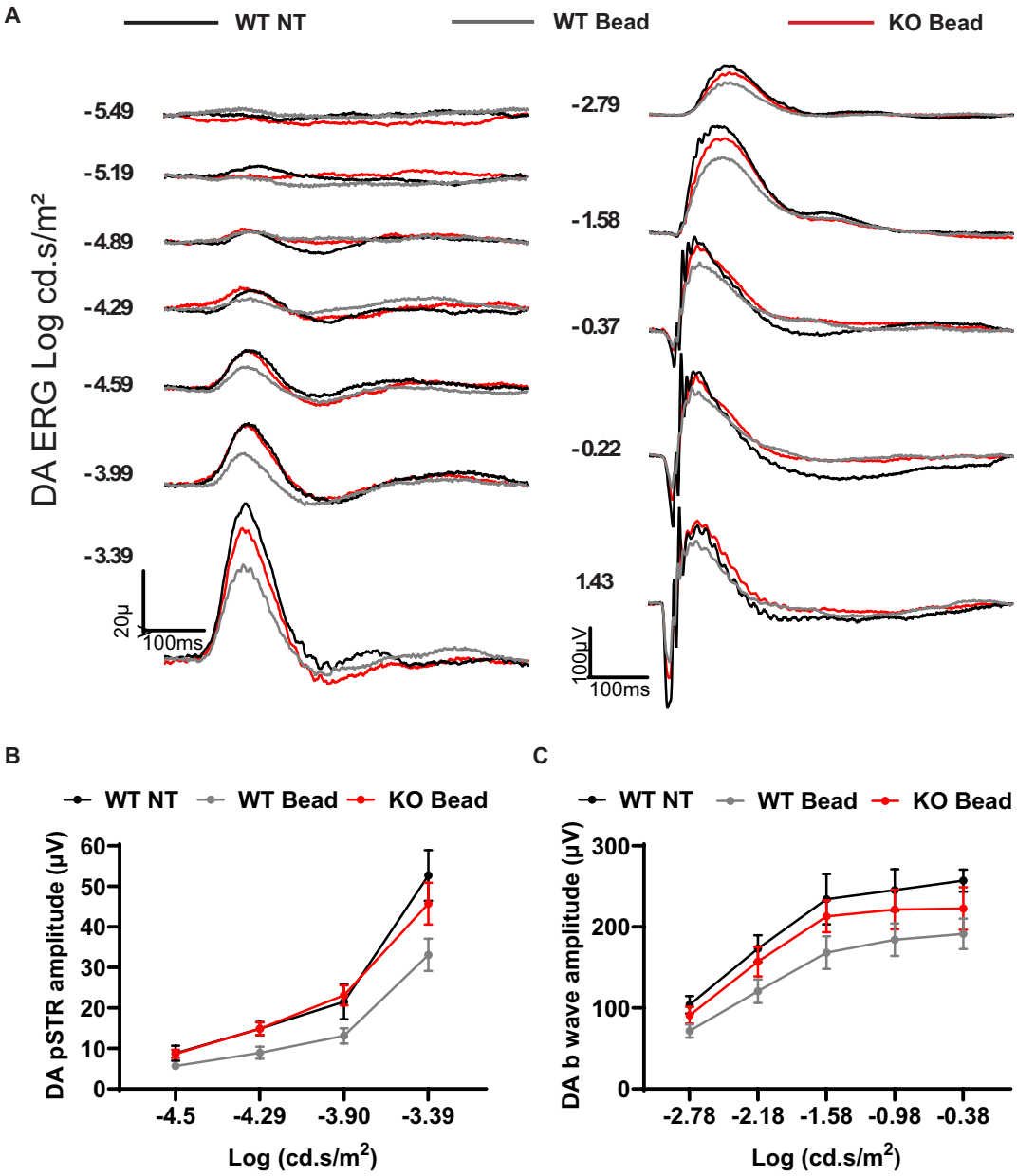

FIGURE 6 | Absence of astrocytic Cx43 preserves visual function in glaucoma. (A) Representative ERG waveforms of bead-injected WT (gray) and Cx43KO (red) mice in comparison to naive control mice (black; non-treated (NT)) at 8 weeks after IOP elevation. (B) Dark-adapted pSTR amplitudes were reduced in bead-injected WT mice compared to naïve control ($n = 9$, $p = 0.0008$). Conditional deletion of Cx43 in astrocytes restored RGC function at 8 weeks after glaucomatous injury ($n = 9$, $p = 0.0002$). (C) b-wave amplitudes were reduced in bead-injected WT mice ($n = 9$, $p = 0.0007$). The absence of Cx43 in astrocytes significantly improved b-wave amplitudes ($n = 9$, $p = 0.01$). Two-way ANOVA, followed by Tukey's test.

and evaluated the effect of Cx43 deletion in astrocytes on RGC survival and on glial changes. ONC induced ~80% RGC loss 7 days after injury ($n = 7$, $p < 0.0001$) while the absence of Cx43 in astrocytes increased RGC survival by two-fold ($n = 8$, $p < 0.001$) (Figure 10C). Cx43 expression in the retina is increased significantly (Cx43 puncta number is increased by 77% and Cx43% area by 2-fold) after ONC compared to control eyes ($n = 7$, $p < 0.001$) (Figure 11C–E).

Deletion of Cx43 did not affect GFAP expression, as it is increased by 20%–25% in both WT (GFAP % area WT ONC eye: 16.41 ± 0.96 vs. control eye: 12.93 ± 0.75, $n = 7$, $p < 0.001$) and Cx43KO mice (GFAP % area Cx43KO ONC eye: 16.85 ± 0.81 vs. control eye: 14.06 ± 0.59, $n = 8$, $p < 0.01$) after ONC. There was no significant difference between WT and Cx43KO after ONC ($p = 0.72$) (Figure 11F).

Furthermore, we assessed gene transcripts of reactive astrocytes following ONC injury. The expressions of several genes were upregulated in WT mice: pan-reactive GFAP (by 3.7-fold), A1 neurotoxic astrocyte genes H2-T23 (by 3.4-fold), Serping1 (by 2.4-fold) and A2 neuroprotective gene S100a10 (by 2-fold). Deletion of Cx43 in astrocytes did not alter gene expression levels of A1 and A2 reactive astrocytes as the upregulation

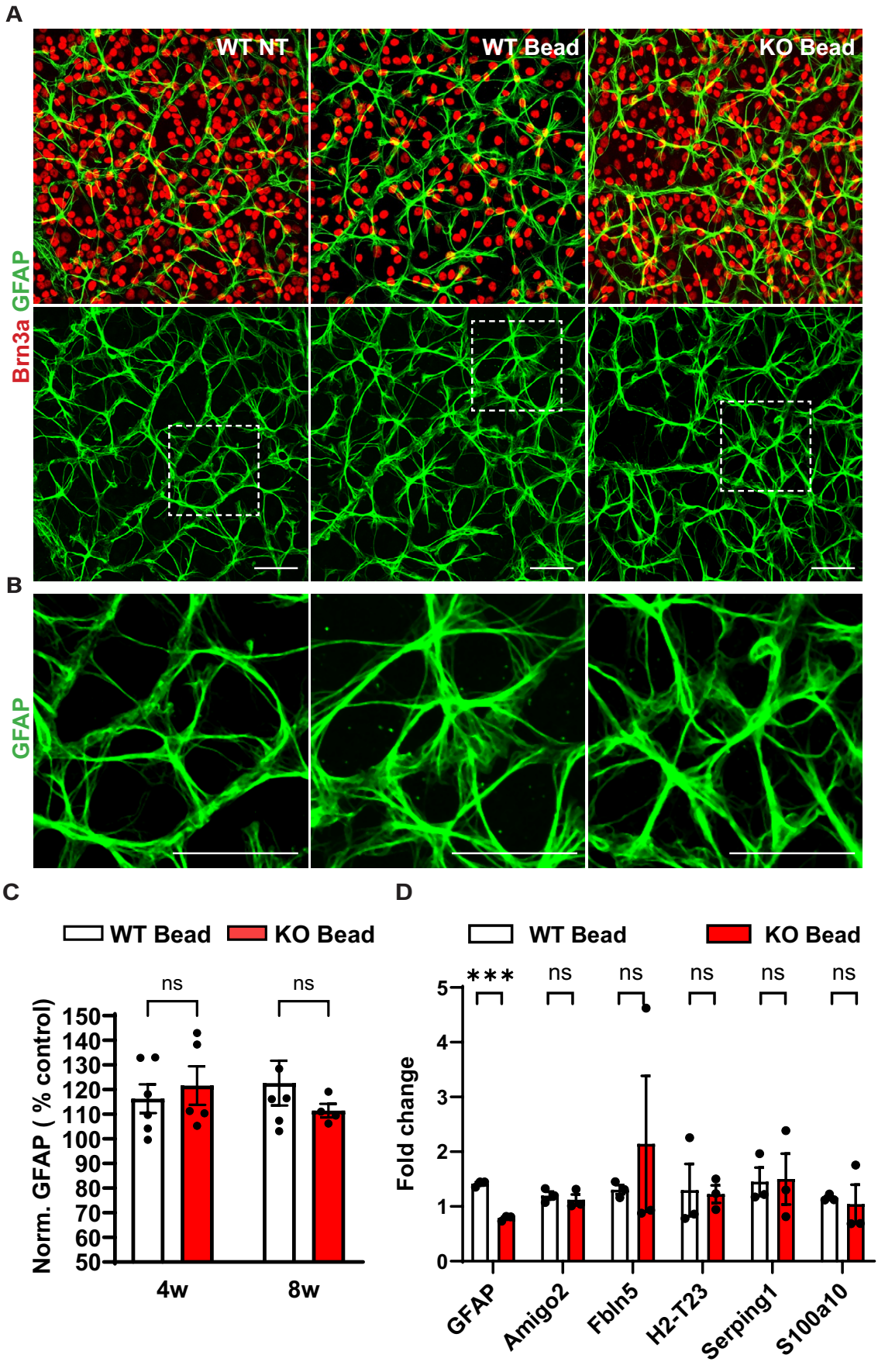

FIGURE 7 | Legend on next page.

FIGURE 7 | Astrocytic reactivity is not affected by deletion of Cx43 in astrocytes. (A) Representative images of control (left; non-treated (NT)) and bead-injected retina of WT (middle) and KO (right) mice 8 weeks after elevated IOP. (B) Magnified sections of selected areas in panel A are shown. (C) Quantification of GFAP-positive area normalized to control indicates that astrocytic reactivity is increased in both WT and KO mice after sustained IOP elevation. (D) Gene transcription analysis of select pan, A1, and A2 reactive astrocytes in injured retina of WT and Cx43KO mice 4 weeks after IOP elevation. The GFAP transcript was upregulated by ~40% in WT mice but was significantly reduced in Cx43KO mice ($n = 3$, $p < 0.001$). A1 and A2 reactive astrocyte gene transcripts are slightly upregulated in both WT and Cx43KO mice in glaucoma, with no significant difference between the groups. ns, not significant, ***$p < 0.001$, Student's t test. Scale bar 50 μm.

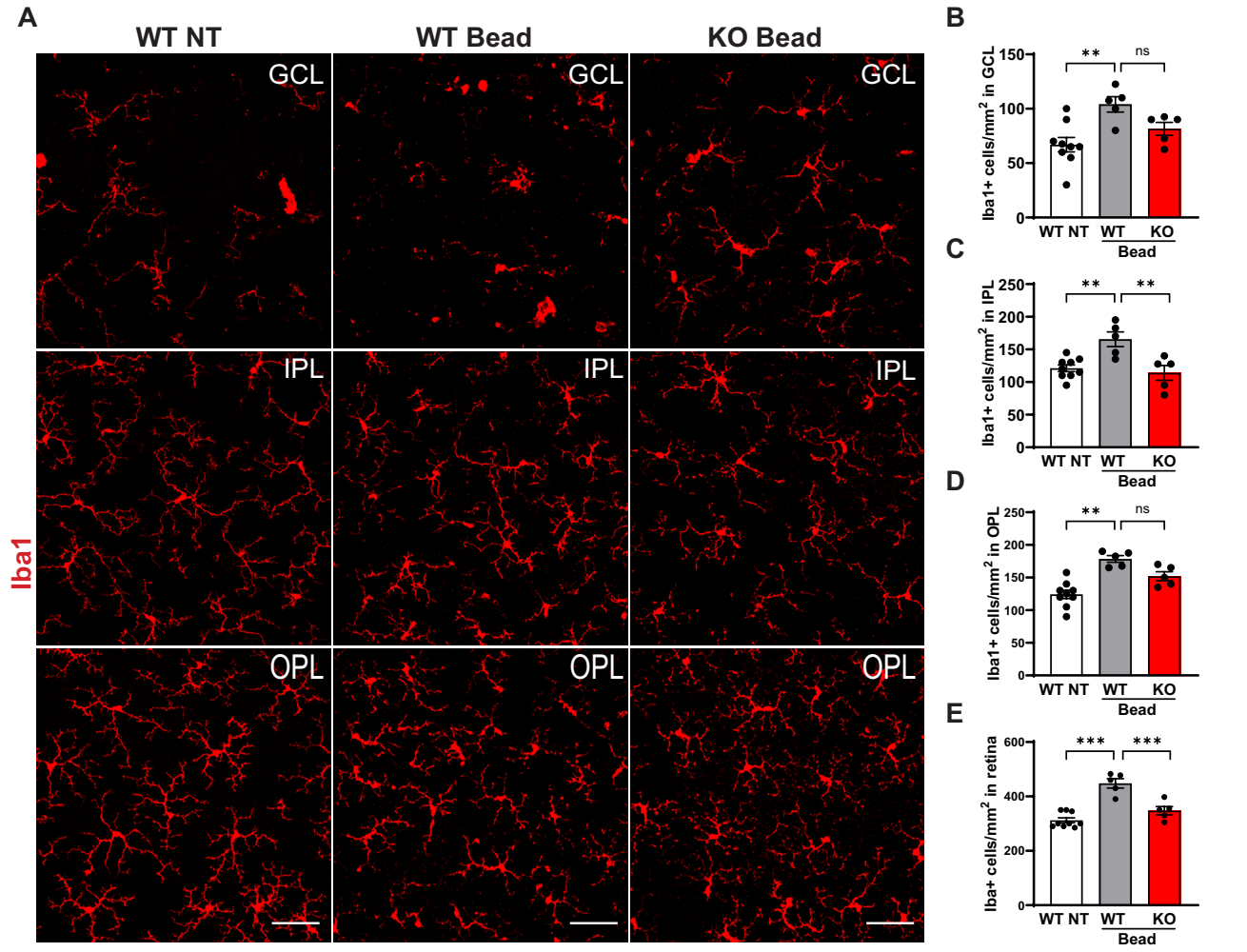

FIGURE 8 | Absence of Cx43 in astrocytes reduces microgliosis. (A) Representative images of Iba1 + microglia/macrophages 8 weeks after bead injection. Quantification of Iba1 + cells in GCL (B), IPL (C), and OPL (D). (E) Quantification of Iba1 + cells in whole retina (GCL + IPL + OPL) after glaucomatous injury shows that the number of microglia is reduced in Cx43KO mice. ns, not significant, *$p < 0.05$, **$p < 0.01$, ***$p < 0.001$, One-way ANOVA, followed by Tukey's test. Scale bar 50 μm.

of these gene transcripts was similar to that of WT mice after ONC. However, GFAP expression was significantly higher in Cx43KO mice than in WT mice after ONC ($n = 4$, $p < 0.05$) (Figure 11G).

3.9 | Application of Gap19 Peptide Is Neuroprotective and Preserves RGC Function

As mentioned previously, Cx43 can form not only GJ channels but can also exist as hemichannels, especially in pathological conditions. Deletion of Cx43 in astrocytes abrogates both GJ coupling and hemichannel activity. To determine whether open Cx43 hemichannels vs. increased GJ channel conductance might contribute to RGC death, we used an inhibitor of hemichannels. Gap19, a peptide derived from the cytoplasmic loop of Cx43, was previously shown to inhibit hemichannels without affecting GJ coupling (Abudara et al. 2014; Wang et al. 2013) Although neither Gap19's potency nor off-target effects have been investigated, the peptide has been used in a number of in vivo and in vitro studies to show the potential contribution of Cx43 hemichannels to disease processes (Chen et al. 2019; Contreras et al. 2002; Danesh-Meyer et al. 2012; Davidson et al. 2013a; Froger et al. 2010; Kang et al. 2008;

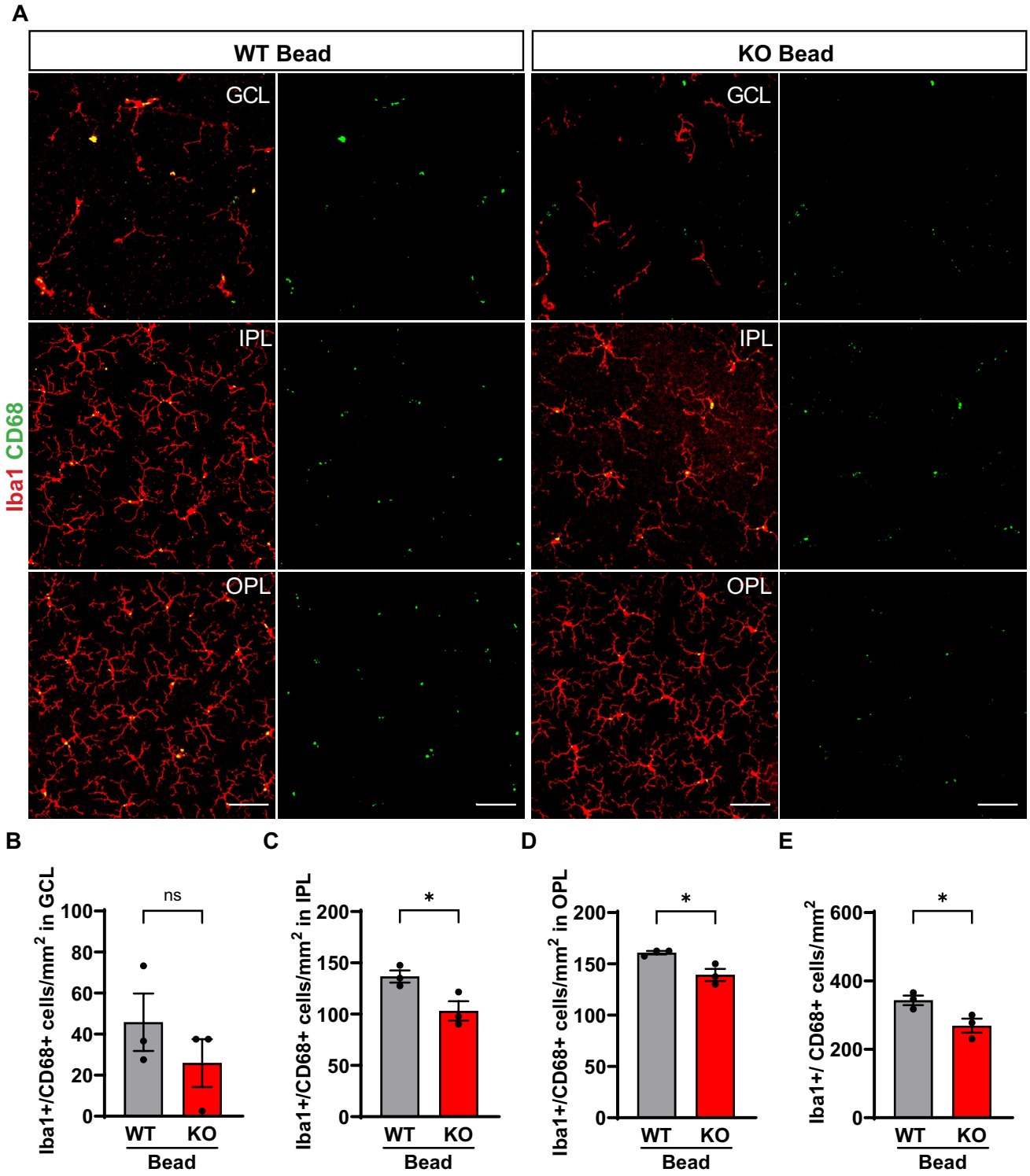

FIGURE 9 | Deletion of Cx43 in astrocytes reduces active phagocytic cells in glaucoma. (A) CD68 expression in Iba1 + microglia/macrophages 8 weeks after bead injection in WT (left) and Cx43KO (right) mice. Quantification of Iba1 +/CD68 + cells in GCL (B), IPL (C), and OPL (D). (E) Quantification of Iba1 +/CD68 + cells in whole retina (GCL + IPL + OPL) shows reduced phagocytic cells in Cx43KO mice after glaucomatous injury. ns, not significant, $^*p < 0.05$, Student's *t* test. Scale bar 50 μm.

Orellana et al. 2011). Gap19 was injected intravitreally every 2 weeks (final concentration in the vitreous 200 μM) for 8 weeks starting from the 2nd week of initial bead injection. RGC survival was evaluated and pSTR amplitude was measured using dark-adapted ERG 8 weeks after IOP elevation (Figure 12). Additionally, astrocytic reactivity (GFAP-positive area) and Cx43 expression (Figure S3) were assessed at 8 weeks after IOP elevation. Gap19 did not affect the increase in Cx43 expression (Figure S3C,D) or astrocyte reactivity (Figure S3B) seen after chronic elevation of IOP ($n = 4$, $p < 0.001$).

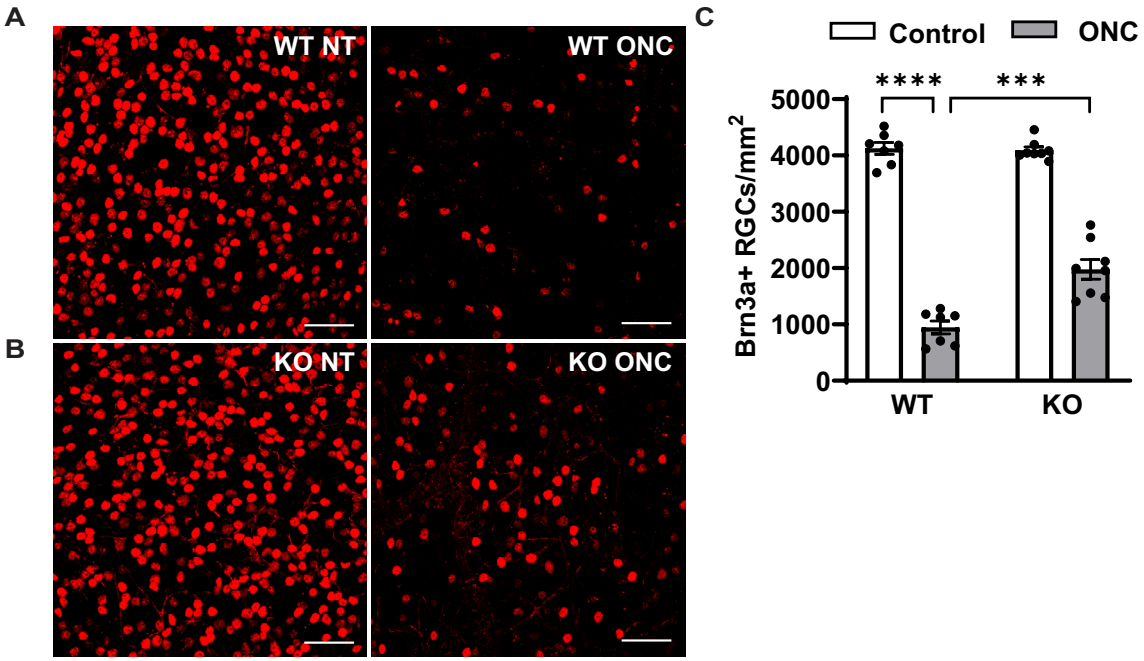

FIGURE 10 | Cx43 deletion is neuroprotective in the optic nerve crush model. (A) Representative images of nontreated control (left) and ONC (right) retinas of WT mice. (B) Representative images of nontreated control (left) and ONC (right) retinas of Cx43KO mice. (C) Quantification of Brn3a + RGCs after ONC in WT and Cx43KO mice. Deletion of Cx43 increases RGC survival by 2-fold. ns, not significant, ***$p < 0.001$, ****$p < 0.0001$, Student's t test. Scale bar 50 μm.

Intravitreal injections of Gap19 at early time points following IOP elevation (i.e., at 2 weeks) were found to be neuroprotective, with Brn3a + RGC survival increasing to ~91% compared to contralateral controls (~69%) ($n = 4$, $p < 0.01$) (Figure 12A,B). In addition, the pSTR amplitude recovered to control levels following Gap19 treatment ($n = 4$, $p < 0.001$) (Figure 12E), indicating preserved visual function in the presence of elevated IOP. To examine whether injections of Gap19 at later time points after RGC loss had commenced can confer neuroprotection, we administered biweekly injections of Gap19 starting from the 4th week after microbead injection. Gap19 injections at this later time point of IOP elevation result in lesser RGC survival (~80%) (Figure 12B) compared to earlier treatment (91%) of Gap19, suggesting that the peptide prevents loss of RGCs despite continued IOP elevation.

We also used a TAT-Gap19 peptide for which a control, scrambled peptide is available commercially. We injected separate groups of mice with TAT-Gap19 and control TAT-Gap19 peptide in one eye and evaluated RGC loss compared to the respective contralateral eye. We found significant protection in the eyes injected with TAT-Gap19 compared to those injected with scrambled peptide (Figure 12D), confirming the effects are specific to Gap19. Treatment with the TAT-Gap19 hemichannel blocker increased RGC survival to 89% compared to control peptide-injected mice ($n = 3$, $p < 0.05$) (Figure 12D). These results suggest that Cx43 hemichannel opening contributes to RGC loss in glaucoma. However, it must be noted that the specificity of Gap19, including off-target effects involving other channels and processes, has not been thoroughly studied, and thus it is possible that these neuroprotective actions are not solely due to Cx43 hemichannel inhibition.

4 | Discussion

Previous studies indicated that deletion of Cx36, the protein that couples RGCs among other cell types in the retina, provides neuroprotection through a bystander effect (Akopian et al. 2017, 2019). This effect purportedly involves the spread of as-yet-unidentified damaging signals throughout the GJ network, culminating in the death of multiple RGCs. Our results described here indicate an independent role for glial connexin channels in glaucoma progression. We demonstrate that Cx43 expression and function are increased in response to sustained elevation of IOP. Genetic deletion of Cx43 in astrocytes promotes RGC survival and restores visual function in the microbead occlusion model of glaucoma. The absence of Cx43 in astrocytes also reduces microglia/macrophage activation in the retina.

Elevation of IOP strongly increases Cx43 expression and GJ coupling, consistent with previous studies showing that Cx43 expression is augmented in the retina and ONH of human patients with glaucoma (Kerr et al. 2011). Similarly, (Cooper et al. 2020) showed that astrocytic coupling is increased 1 week after IOP elevation after microbead injection. Our finding that Cx43 expression and GJ coupling are increased 4 and 8 weeks after elevated IOP indicates that Cx43 expression is altered soon after the initiation of injury and persists for an extended period of time, contributing to disease progression. We also found that astrocytes are coupled to Müller cells in the mouse retina, as in rabbit and rat retinas (Robinson et al. 1993; Zahs and Newman 1997). The coupling between astrocytes and Müller cells is strengthened by chronic elevation of IOP, increasing the coupled Müller cells by ~3.8-fold. Furthermore, we showed that Müller cells were not coupled to each other, and they were not affected by

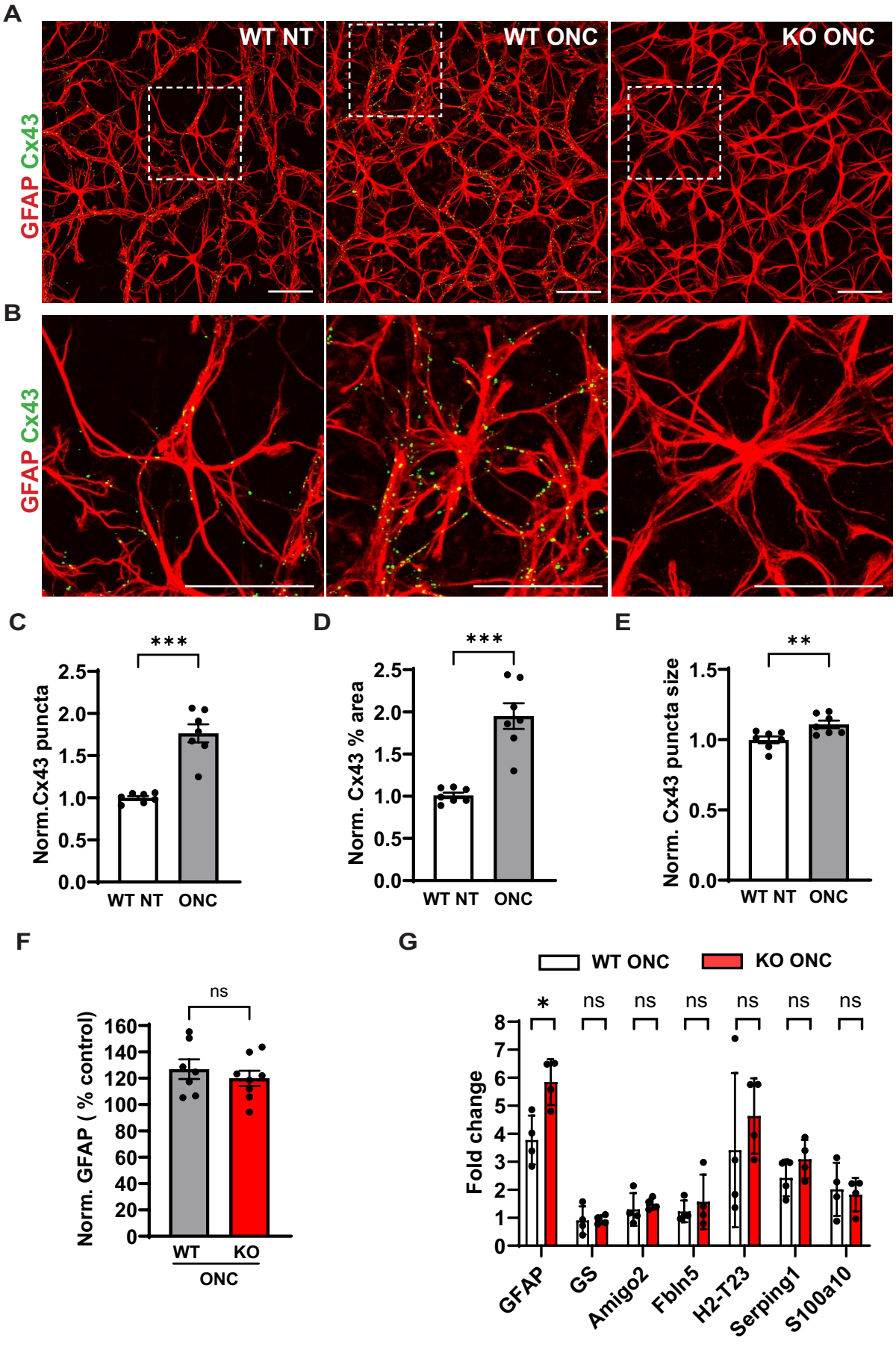

FIGURE 11 | Legend on next page.

FIGURE 11 | Deletion of Cx43 in astrocytes does not affect reactivity of astrocytes after ONC injury. (A) Representative images of control (left) and WT (middle) and Cx43KO (right) mice 7 days after ONC. (B) Magnified sections of selected areas in panel A are shown. (C–E) Cx43 expression (count, size, percent area) is increased in WT mice after ONC. (F) Quantification of the GFAP-positive area normalized to controls shows that astrocytic reactivity is similarly increased in WT and KO mice after ONC injury. (G) Gene transcription analysis of select pan, A1, and A2 reactive astrocytes in WT and Cx43KO mice 7 days after ONC injury. Gene expression levels of A1 and A2 reactive astrocytes are increased in both WT and Cx43KO mice after ONC. GFAP transcript level was higher in injured retinas of Cx43KO mice than WT mice. *$p < 0.05$, **$p < 0.01$, ***$p < 0.001$. Student's t test. Scale bar 50 μm.

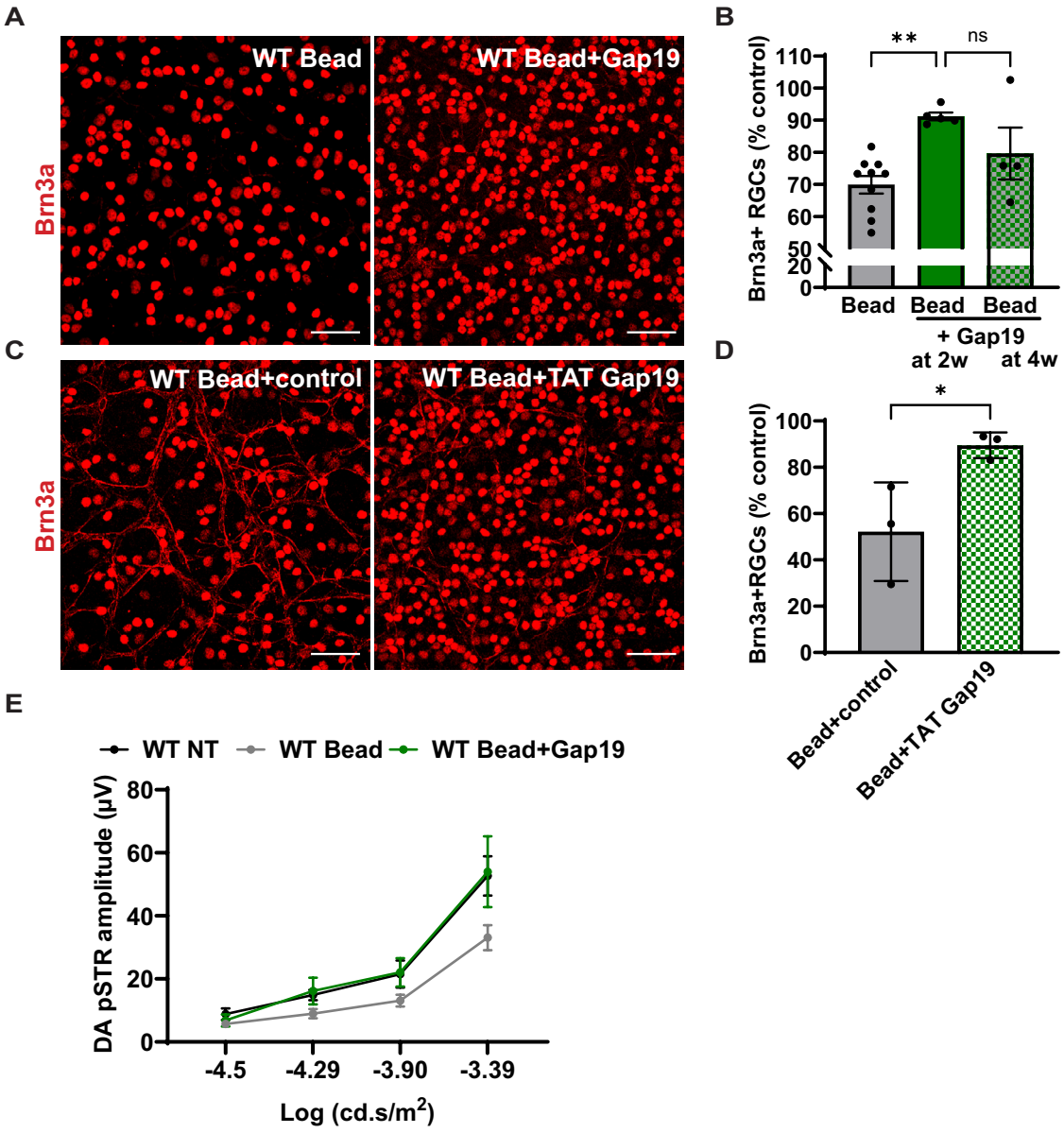

FIGURE 12 | Inhibition of Cx43 hemichannel activity is neuroprotective and preserves RGC function in glaucoma. (A) Representative images of (glaucomatous WT with no treatment (left) and with intravitreally injected Gap19 (right). (B) Quantification of Brn3a (+) RGCs after Gap19 treatment in glaucomatous mice. Gap19 was injected intravitreally every 2 weeks for 8 weeks starting from either the 2nd or 4th weeks after initial microbead injection. Gap-19 treatment beginning at 2 weeks improves RGC survival to ~90% ($n = 4$, $p < 0.01$) compared to nontreated glaucomatous mice (~69%). Gap19 treatment at 4 weeks after IOP elevation results in lesser (80%) RGC survival ($n = 4$). (C) Representative images of glaucomatous WT with TAT-Gap19 control peptide (left) and TAT-Gap19 (right) treatments. TAT-Gap19 control peptide and TAT-Gap19 were intravitreally injected for 8 weeks starting from the 2nd week of initial bead injection. (D) Quantification of Brn3a + RGCs in glaucomatous mice shows TAT-Gap19 treatment promotes RGC survival ($n = 3$, $p < 0.05$) significantly more than the control peptide ($n = 3$). (E) Quantification of pSTR amplitudes shows Gap19 treatment preserves RGC function ($n = 4$, $p < 0.001$). ns, not significant, *$p < 0.05$, **$p < 0.01$, Student's t test, One- and Two-way ANOVA, followed by Tukey's test. Scale bar 50 μm.

IOP elevation, indicating that the increase of NB + Müller cells is due to increased coupling between astrocytes.

Previously, we reported that conditional deletion of Cx43 in astrocytes does not affect normal retinal physiology (Slavi et al. 2018; Toychiev et al. 2021). However, we find that Cx43 deletion in astrocytes reduces RGC loss and preserves visual function, indicating that Cx43 has a deleterious effect on neuronal survival after sustained IOP elevation (at 4 and 8 weeks). In contrast, the role of Cx43 in early glaucomatous injury (1–2 weeks) (Cooper et al. 2020) in unilateral conditions wherein IOP was elevated in one eye indicated a neuroprotective role for astrocytic Cx43. This study showed that when retinas are subjected to unilateral stress, redistribution of glycogen-derived bioenergetic resources can occur from unstressed contralateral eyes to injured eyes and promote tissue survival through astrocytic Cx43 GJs (Cooper et al. 2020). Cx43 deletion induced greater damage to the injured eye without metabolic support from the uninjured eye. The effects of Cx43KO on RGC loss or visual function at later time points were not examined. We hypothesize that these differing results occur because astrocytes exhibit neuroprotective effects in early stages of injury, whereas their neurotoxic effects predominate with chronic injury.

Our hypothesis above is consistent with a number of studies that demonstrate that the overall impact of reactive astrocytes on neuronal function varies with disease severity and duration and can either lead to beneficial or deleterious clinical outcomes (Bayraktar et al. 2020; John Lin et al. 2017; Liddelow et al. 2017; Rothhammer et al. 2018; Wheeler et al. 2020). Astrocyte reactivity in early disease stages mediates neuroprotective effects in glaucoma and other CNS diseases (Anderson et al. 2016; Calkins 2021; Khakh and Sofroniew 2015; Livne-Bar et al. 2017; Mayo et al. 2014; Okada et al. 2006; Sun et al. 2017). Attenuation of astrocyte reactivity in the ONH, an early site of damage in glaucomatous injury, caused a decrease in RGC viability and accelerated visual impairment in glaucoma and ONC (Sun et al. 2017). In contrast, reactive astrocytes in chronic injury settings actively promote inflammation and contribute to the pathogenesis of neurodegenerative diseases, including glaucoma (Barakat et al. 2012; Brambilla et al. 2014; Dvoriantchikova et al. 2009; Livne-Bar et al. 2016; Rothhammer and Quintana 2019; Tezel 2008; Wheeler et al. 2020; Yang et al. 2020).

This hypothesis ties with a finding of our study suggesting that the inhibition of hemichannels was neuroprotective in this model of glaucoma. Intravitreal injections of Gap19 peptide for the duration of IOP elevation markedly increased RGC survival and improved RGC function, without affecting the expression of Cx43 in astrocytes. The degree of neuroprotection was similar to that found in Cx43KO mice, indicating that the detrimental effect of Cx43 is possibly through activated hemichannels, although additional studies are essential because the peptide could have effects on other cellular processes when used in vivo. These results indicate that astrocytes in chronic injury settings might increase Cx43 hemichannel activity and actively promote neuronal death in glaucoma. The opening of Cx43 hemichannels is known to release ATP, glutamate, and other mediators (Contreras et al. 2002; Danesh-Meyer et al. 2012; Davidson et al. 2013a; Froger et al. 2010; Kang et al. 2008; Orellana et al. 2011). In addition, the release of proinflammatory cytokines such as tumor necrosis factor (TNF)-α and interleukin 1β, which is known to occur in glaucoma (Balaiya et al. 2011; Madeira et al. 2015; Nakazawa et al. 2006; Neufeld 1999; Sawada et al. 2010; Wilson et al. 2015) can further activate Cx43 hemichannels. Since Cx43 hemichannels are not active in physiological conditions, future studies using agents that are highly specific for hemichannels might provide a promising strategy for the treatment of glaucoma.

Both Cx43 hemichannel activity and GJ coupling have been implicated in neurodegenerative diseases (Frantseva et al. 2002; Freitas-Andrade et al. 2019; Lin et al. 1998; Rami et al. 2001) and retinal injuries (Danesh-Meyer et al. 2012; Slavi et al. 2018; Toychiev et al. 2021). Our data suggest that elevated IOP increases both hemichannel activity and cell-to-cell communication of astrocytes. These results are consistent with a recent in vivo study (Freitas-Andrade et al. 2019) showing that both astrocytic Cx43 coupling and hemichannel activity are increased following ischemia in the brain. In addition, this study showed that inhibition of MAPK phosphorylation (Ser 255/262/279/282A) reduced hemichannel activity but not GJ coupling in hypoxia and reduced infarct volume and functional deficits after stroke (Freitas-Andrade et al. 2019). Whether similar changes in phosphorylation status of Cx43 occur in glaucoma, causing increases in hemichannel activity, remains to be determined.

Activation of microglia is one of the earliest changes in glaucoma (Bosco et al. 2011; Kumar et al. 2023) and the degree of microgliosis correlates with the magnitude of axonal loss (Bosco et al. 2016; Ebneter et al. 2010). Microglial activation is a complex process that includes proliferation, morphological changes, branching and retraction of processes, expression of phagocytic markers, and production of proinflammatory cytokines. Consistent with previous studies (Bosco et al. 2011; Kumar et al. 2023; Neufeld 1999; Tribble et al. 2020), we observed changes in microglial density and morphology 8 weeks after bead injection. Prolonged elevation of IOP increased the number of microglia as well as CD68 + phagocytic cells in all retinal layers, including OPL. Activation of microglia in OPL may be due to secondary damage of the outer retina, as previously reported (Cuenca et al. 2010; Fernandez-Sanchez et al. 2014; Hernandez et al. 2009; Kumar et al. 2021; Pang et al. 2015; Velten et al. 2001). Deletion of Cx43 resulted in lower microglial density and a reduced number of active phagocytic cells in the retina in both IPL and OPL. It is likely that reduced microglial activation might be due to a decrease in neuronal death provided by Cx43 deletion in astrocytes. Damaged neurons can release nucleotides (Koizumi et al. 2007; Ohsawa et al. 2007; Wu et al. 2007), HMGB1 protein (Chi et al. 2015; Nakazawa et al. 2006), and heat shock proteins (Tezel and Fourth 2009), which affect purinergic, CD11, and TLR signaling in microglia and lead to an increase in their phagocytic ability and production of proinflammatory cytokines. Furthermore, ATP released from astrocytes through connexin hemichannels is known to stimulate microglial activation, which was abrogated by ATPase and channel inhibitors. Thus, deletion of Cx43 likely contributes to the reduction of microglial reactivity via a Cx43-hemichannel mediated mechanism (Davalos et al. 2005).

Author Contributions

K.B. designed and performed majority of the experiments, collected and analyzed data and wrote the manuscript. M.S. designed experiments and helped write the manuscript. A.H.T. performed the dye transfer studies and read the manuscript. S.V. helped with ERG studies and ERG data analysis. S.G.W. designed the qPCR studies, established methods for data anlaysis and aided in interpretation of the data.

Ethics Statement

The SUNY College of Optometry Institutional Animal Care and Use Committee approved the experimental procedures utilized in this study.

Conflicts of Interest

The authors declare no conflicts of interest.

Data Availability Statement

The data that support the findings of this study are available from the corresponding author upon reasonable request.

References

Abudara, V., J. Bechberger, M. Freitas-Andrade, et al. 2014. "The Connexin 43 Mimetic Peptide Gap19 Inhibits Hemichannels Without Altering Gap Junctional Communication in Astrocytes." *Frontiers in Cellular Neuroscience* 8: 306. https://doi.org/10.3389/fncel.2014.00306.

Akopian, A., S. Kumar, H. Ramakrishnan, K. Roy, S. Viswanathan, and S. A. Bloomfield. 2017. "Targeting Neuronal Gap Junctions in Mouse Retina Offers Neuroprotection in Glaucoma." *Journal of Clinical Investigation* 127: 2647–2661.

Akopian, A., S. Kumar, H. Ramakrishnan, S. Viswanathan, and S. A. Bloomfield. 2019. "Amacrine Cells Coupled to Ganglion Cells via Gap Junctions Are Highly Vulnerable in Glaucomatous Mouse Retinas." *Journal of Comparative Neurology* 527: 159–173.

Anderson, M. A., J. E. Burda, Y. Ren, et al. 2016. "Astrocyte Scar Formation Aids Central Nervous System Axon Regeneration." *Nature* 532, no. 7598: 195–200. https://doi.org/10.1038/nature17623.

Balaiya, S., J. Edwards, T. Tillis, V. Khetpal, and K. V. Chalam. 2011. "Tumor Necrosis Factor-Alpha (TNF-Alpha) Levels in Aqueous Humor of Primary Open Angle Glaucoma." *Clinical Ophthalmology* 5: 553–556.

Barakat, D. J., G. Dvoriantchikova, D. Ivanov, and V. I. Shestopalov. 2012. "Astroglial NF-KappaB Mediates Oxidative Stress by Regulation of NADPH Oxidase in a Model of Retinal Ischemia Reperfusion Injury." *Journal of Neurochemistry* 120: 586–597.

Bayer, A. U., T. Neuhardt, A. C. May, et al. 2001. "Retinal Morphology and ERG Response in the DBA/2NNia Mouse Model of Angle-Closure Glaucoma." *Investigative Ophthalmology & Visual Science* 42: 1258–1265.

Bayraktar, O. A., T. Bartels, S. Holmqvist, et al. 2020. "Astrocyte Layers in the Mammalian Cerebral Cortex Revealed by a Single-Cell In Situ Transcriptomic Map." *Nature Neuroscience* 23: 500–509.

Bennett, M. V., J. M. Garre, J. A. Orellana, F. F. Bukauskas, M. Nedergaard, and J. C. Saez. 2012. "Connexin and Pannexin Hemichannels in Inflammatory Responses of Glia and Neurons." *Brain Research* 1487: 3–15.

Bosco, A., K. T. Breen, S. R. Anderson, M. R. Steele, D. J. Calkins, and M. L. Vetter. 2016. "Glial Coverage in the Optic Nerve Expands in Proportion to Optic Axon Loss in Chronic Mouse Glaucoma." *Experimental Eye Research* 150: 34–43.

Bosco, A., M. R. Steele, and M. L. Vetter. 2011. "Early Microglia Activation in a Mouse Model of Chronic Glaucoma." *Journal of Comparative Neurology* 519: 599–620.

Brambilla, R., P. D. Morton, J. J. Ashbaugh, S. Karmally, K. L. Lambertsen, and J. R. Bethea. 2014. "Astrocytes Play a Key Role in EAE Pathophysiology by Orchestrating in the CNS the Inflammatory Response of Resident and Peripheral Immune Cells and by Suppressing Remyelination." *GLIA* 62: 452–467.

Calder, B. W., J. Matthew Rhett, H. Bainbridge, S. A. Fann, R. G. Gourdie, and M. J. Yost. 2015. "Inhibition of Connexin 43 Hemichannel-Mediated ATP Release Attenuates Early Inflammation During the Foreign Body Response." *Tissue Engineering. Part A* 21: 1752–1762.

Calkins, D. J. 2021. "Adaptive Responses to Neurodegenerative Stress in Glaucoma." *Progress in Retinal and Eye Research* 84: 100953.

Chen, B., L. Yang, J. Chen, et al. 2019. "Inhibition of Connexin 43 Hemichannels With Gap19 Protects Cerebral Ischemia/Reperfusion Injury via the JAK2/STAT3 Pathway in Mice." *Brain Research Bulletin* 146: 124–135.

Chen, H., X. Wei, K. S. Cho, et al. 2011. "Optic Neuropathy due to Microbead-Induced Elevated Intraocular Pressure in the Mouse." *Investigative Ophthalmology & Visual Science* 52: 36–44.

Chi, W., H. Chen, F. Li, Y. Zhu, W. Yin, and Y. Zhuo. 2015. "HMGB1 Promotes the Activation of NLRP3 and Caspase-8 Inflammasomes via NF-kappaB Pathway in Acute Glaucoma." *Journal of Neuroinflammation* 12: 137.

Chidlow, G., A. Ebneter, J. P. Wood, and R. J. Casson. 2016. "Evidence Supporting an Association Between Expression of Major Histocompatibility Complex II by Microglia and Optic Nerve Degeneration During Experimental Glaucoma." *Journal of Glaucoma* 25: 681–691.

Contreras, J. E., J. C. Saez, F. F. Bukauskas, and M. V. Bennett. 2003. "Gating and Regulation of Connexin 43 (Cx43) Hemichannels." *Proceedings of the National Academy of Sciences of the United States of America* 100: 11388–11393.

Contreras, J. E., H. A. Sanchez, E. A. Eugenin, et al. 2002. "Metabolic Inhibition Induces Opening of Unapposed Connexin 43 Gap Junction Hemichannels and Reduces Gap Junctional Communication in Cortical Astrocytes in Culture." *Proceedings of the National Academy of Sciences of the United States of America* 99: 495–500.

Cooper, M. L., S. Pasini, W. S. Lambert, et al. 2020. "Redistribution of Metabolic Resources Through Astrocyte Networks Mitigates Neurodegenerative Stress." *Proceedings of the National Academy of Sciences of the United States of America* 117, no. 31: 18810–18821. https://doi.org/10.1073/pnas.2009425117.

Cuenca, N., I. Pinilla, L. Fernandez-Sanchez, et al. 2010. "Changes in the Inner and Outer Retinal Layers After Acute Increase of the Intraocular Pressure in Adult Albino Swiss Mice." *Experimental Eye Research* 91: 273–285.

Danesh-Meyer, H. V., N. M. Kerr, J. Zhang, et al. 2012. "Connexin 43 Mimetic Peptide Reduces Vascular Leak and Retinal Ganglion Cell Death Following Retinal Ischaemia." *Brain: A Journal of Neurology* 135: 506–520.

Davalos, D., J. Grutzendler, G. Yang, et al. 2005. "ATP Mediates Rapid Microglial Response to Local Brain Injury In Vivo." *Nature Neuroscience* 8, no. 6: 752–758. https://doi.org/10.1038/nn1472.

Davidson, J. O., C. R. Green, L. Bennet, et al. 2013a. "A Key Role for Connexin Hemichannels in Spreading Ischemic Brain Injury." *Current Drug Targets* 14: 36–46.

Davidson, J. O., C. R. Green, L. F. Nicholson, L. Bennet, and A. J. Gunn. 2013b. "Connexin Hemichannel Blockade Is Neuroprotective After, but Not During, Global Cerebral Ischemia in Near-Term Fetal Sheep." *Experimental Neurology* 248: 301–308.

Dvoriantchikova, G., D. Barakat, R. Brambilla, et al. 2009. "Inactivation of Astroglial NF-Kappa B Promotes Survival of Retinal Neurons Following Ischemic Injury." *European Journal of Neuroscience* 30, no. 2: 175–185. https://doi.org/10.1111/j.1460-9568.2009.06814.x.

Ebneter, A., R. J. Casson, J. P. Wood, and G. Chidlow. 2010. "Microglial Activation in the Visual Pathway in Experimental Glaucoma: Spatiotemporal Characterization and Correlation With Axonal Injury." *Investigative Ophthalmology & Visual Science* 51: 6448–6460.

Escartin, C., E. Galea, A. Lakatos, et al. 2021. "Reactive Astrocyte Nomenclature, Definitions, and Future Directions." *Nature Neuroscience* 24, no. 3: 312–325. https://doi.org/10.1038/s41593-020-00783-4.

Fernandez-Sanchez, L., L. P. de Sevilla Muller, N. C. Brecha, and N. Cuenca. 2014. "Loss of Outer Retinal Neurons and Circuitry Alterations in the DBA/2J Mouse." *Investigative Ophthalmology & Visual Science* 55: 6059–6072.

Foster, P. J., R. Buhrmann, H. A. Quigley, and G. J. Johnson. 2002. "The Definition and Classification of Glaucoma in Prevalence Surveys." *British Journal of Ophthalmology* 86: 238–242.

Frantseva, M. V., L. Kokarovtseva, and J. L. Perez Velazquez. 2002. "Ischemia-Induced Brain Damage Depends on Specific Gap-Junctional Coupling." *Journal of Cerebral Blood Flow and Metabolism: Official Journal of the International Society of Cerebral Blood Flow and Metabolism* 22: 453–462.

Freitas-Andrade, M., N. Wang, J. F. Bechberger, et al. 2019. "Targeting MAPK Phosphorylation of Connexin 43 Provides Neuroprotection in Stroke." *Journal of Experimental Medicine* 216: 916–935.

Froger, N., J. A. Orellana, C. F. Calvo, et al. 2010. "Inhibition of Cytokine-Induced Connexin 43 Hemichannel Activity in Astrocytes Is Neuroprotective." *Molecular and Cellular Neurosciences* 45: 37–46.

Gajardo-Gómez, R., V. C. Labra, C. J. Maturana, et al. 2017. "Cannabinoids Prevent the Amyloid β-Induced Activation of Astroglial Hemichannels: A Neuroprotective Mechanism." 65, no. 1: 122–137. https://doi.org/10.1002/glia.23080.

Giulian, D., T. J. Baker, L. C. Shih, and L. B. Lachman. 1986. "Interleukin 1 of the Central Nervous System Is Produced by Ameboid Microglia." *Journal of Experimental Medicine* 164: 594–604.

Guttenplan, K. A., B. K. Stafford, R. N. El-Danaf, et al. 2020. "Neurotoxic Reactive Astrocytes Drive Neuronal Death After Retinal Injury." *Cell Reports* 31: 107776.

Hanisch, U. K. 2002. "Microglia as a Source and Target of Cytokines." *GLIA* 40: 140–155.

Harazny, J., M. Scholz, T. Buder, B. Lausen, and J. Kremers. 2009. "Electrophysiological Deficits in the Retina of the DBA/2J Mouse." *Documenta Ophthalmologica. Advances in Ophthalmology* 119: 181–197.

Hernandez, M., F. D. Rodriguez, S. C. Sharma, and E. Vecino. 2009. "Immunohistochemical Changes in Rat Retinas at Various Time Periods of Elevated Intraocular Pressure." *Molecular Vision* 15: 2696–2709.

Holness, C. L., and D. L. Simmons. 1993. "Molecular Cloning of CD68, a Human Macrophage Marker Related to Lysosomal Glycoproteins." *Blood* 81: 1607–1613.

Huang, Y., Z. Li, N. van Rooijen, N. Wang, C. P. Pang, and Q. Cui. 2007. "Different Responses of Macrophages in Retinal Ganglion Cell Survival After Acute Ocular Hypertension in Rats With Different Autoimmune Backgrounds." *Experimental Eye Research* 85: 659–666.

Isenmann. 1997. "Up-Regulation of Bax Protein in Degenerating Retinal Ganglion Cells Precedes Apoptotic Cell Death After Optic Nerve Lesion in the Rat."

John Lin, C. C., K. Yu, A. Hatcher, et al. 2017. "Identification of Diverse Astrocyte Populations and Their Malignant Analogs." *Nature Neuroscience* 20: 396–405.

Kang, J., N. Kang, D. Lovatt, et al. 2008. "Connexin 43 Hemichannels Are Permeable to ATP." *Journal of Neuroscience: The Official Journal of the Society for Neuroscience* 28: 4702–4711.

Kerr, N. M., C. S. Johnson, C. R. Green, and H. V. Danesh-Meyer. 2011. "Gap Junction Protein Connexin 43 (GJA1) in the Human Glaucomatous Optic Nerve Head and Retina." *Journal of Clinical Neuroscience: Official Journal of the Neurosurgical Society of Australasia* 18: 102–108.

Khakh, B. S., and M. V. Sofroniew. 2015. "Diversity of Astrocyte Functions and Phenotypes in Neural Circuits." *Nature Neuroscience* 18: 942–952.

Koizumi, S., Y. Shigemoto-Mogami, K. Nasu-Tada, et al. 2007. "UDP Acting at P2Y6 Receptors Is a Mediator of Microglial Phagocytosis." *Nature* 446, no. 7139: 1091–1095. https://doi.org/10.1038/nature05704.

Kumar, S., A. Akopian, and S. A. Bloomfield. 2023. "Neuroprotection of Retinal Ganglion Cells Suppresses Microglia Activation in a Mouse Model of Glaucoma." *Investigative Ophthalmology & Visual Science* 64: 24.

Kumar, S., H. Ramakrishnan, S. Viswanathan, A. Akopian, and S. A. Bloomfield. 2021. "Neuroprotection of the Inner Retina Also Prevents Secondary Outer Retinal Pathology in a Mouse Model of Glaucoma." *Investigative Ophthalmology & Visual Science* 62: 35.

Liddelow, S. A., K. A. Guttenplan, L. E. Clarke, et al. 2017. "Neurotoxic Reactive Astrocytes Are Induced by Activated Microglia." *Nature* 541, no. 7638: 481–487. https://doi.org/10.1038/nature21029.

Lin, J. H., H. Weigel, M. L. Cotrina, et al. 1998. "Gap-Junction-Mediated Propagation and Amplification of Cell Injury." *Nature Neuroscience* 1, no. 6: 494–500. https://doi.org/10.1038/2210.

Livne-Bar, I., S. Lam, D. Chan, et al. 2016. "Pharmacologic Inhibition of Reactive Gliosis Blocks TNF-Alpha-Mediated Neuronal Apoptosis." *Cell Death & Disease* 7: e2386.

Livne-Bar, I., J. Wei, H. H. Liu, et al. 2017. "Astrocyte-Derived Lipoxins A4 and B4 Promote Neuroprotection From Acute and Chronic Injury." *Journal of Clinical Investigation* 127: 4403–4414.

Madeira, M. H., R. Boia, P. F. Santos, A. F. Ambrosio, and A. R. Santiago. 2015. "Contribution of Microglia-Mediated Neuroinflammation to Retinal Degenerative Diseases." *Mediators of Inflammation* 2015: 673090.

Madisen, L., T. A. Zwingman, S. M. Sunkin, et al. 2010. "A Robust and High-Throughput Cre Reporting and Characterization System for the Whole Mouse Brain." *Nature Neuroscience* 13: 133–140.

Margeta, M. A., E. M. Lad, and A. D. Proia. 2018. "CD163 + Macrophages Infiltrate Axon Bundles of Postmortem Optic Nerves With Glaucoma." *Graefe's Archive for Clinical and Experimental Ophthalmology = Albrecht von Graefes Archiv Fur Klinische Und Experimentelle Ophthalmologie* 256: 2449–2456.

Mayo, L., S. A. Trauger, M. Blain, et al. 2014. "Regulation of Astrocyte Activation by Glycolipids Drives Chronic CNS Inflammation." *Nature Medicine* 20, no. 10: 1147–1156. https://doi.org/10.1038/nm.3681.

Miller, K. M., and H. A. Quigley. 1988. "The Clinical Appearance of the Lamina Cribrosa as a Function of the Extent of Glaucomatous Optic Nerve Damage." *Ophthalmology* 95: 135–138.

Nakazawa, T., C. Nakazawa, A. Matsubara, et al. 2006. "Tumor Necrosis Factor-Alpha Mediates Oligodendrocyte Death and Delayed Retinal Ganglion Cell Loss in a Mouse Model of Glaucoma." *Journal of Neuroscience: The Official Journal of the Society for Neuroscience* 26: 12633–12641.

Neufeld, A. H. 1999. "Microglia in the Optic Nerve Head and the Region of Parapapillary Chorioretinal Atrophy in Glaucoma." *Archives of Ophthalmology* 117: 1050–1056.

Ohsawa, K., Y. Irino, Y. Nakamura, C. Akazawa, K. Inoue, and S. Kohsaka. 2007. "Involvement of P2X4 and P2Y12 Receptors in ATP-Induced Microglial Chemotaxis." *GLIA* 55: 604–616.

Okada, S., M. Nakamura, H. Katoh, et al. 2006. "Conditional Ablation of Stat3 or Socs3 Discloses a Dual Role for Reactive Astrocytes After Spinal Cord Injury." *Nature Medicine* 12: 829–834.

Orellana, J. A., N. Froger, P. Ezan, et al. 2011. "ATP and Glutamate Released via Astroglial Connexin 43 Hemichannels Mediate Neuronal Death Through Activation of Pannexin 1 Hemichannels." *Journal of Neurochemistry* 118, no. 5: 826–840. https://doi.org/10.1111/j.1471-4159.2011.07210.x.

Orellana, J. A., R. von Bernhardi, C. Giaume, and J. C. Saez. 2012. "Glial Hemichannels and Their Involvement in Aging and Neurodegenerative Diseases." *Reviews in the Neurosciences* 23: 163–177.

Pang, J. J., B. J. Frankfort, R. L. Gross, and S. M. Wu. 2015. "Elevated Intraocular Pressure Decreases Response Sensitivity of Inner Retinal Neurons in Experimental Glaucoma Mice." *Proceedings of the National Academy of Sciences of the United States of America* 112: 2593–2598.

Pekny, M., and M. Pekna. 2014. "Astrocyte Reactivity and Reactive Astrogliosis: Costs and Benefits." *Physiological Reviews* 94: 1077–1098.

Pekny, M., U. Wilhelmsson, and M. Pekna. 2014. "The Dual Role of Astrocyte Activation and Reactive Gliosis." *Neuroscience Letters* 565: 30–38.

Quigley, H. A., E. M. Addicks, W. R. Green, and A. E. Maumenee. 1981. "Optic Nerve Damage in Human Glaucoma. II. The Site of Injury and Susceptibility to Damage." *Archives of Ophthalmology* 99: 635–649.

Rami, A., T. Volkmann, and J. Winckler. 2001. "Effective Reduction of Neuronal Death by Inhibiting Gap Junctional Intercellular Communication in a Rodent Model of Global Transient Cerebral Ischemia." *Experimental Neurology* 170: 297–304.

Retamal, M. A., N. Froger, N. Palacios-Prado, et al. 2007. "Cx43 Hemichannels and Gap Junction Channels in Astrocytes Are Regulated Oppositely by Proinflammatory Cytokines Released From Activated Microglia." *Journal of Neuroscience: The Official Journal of the Society for Neuroscience* 27: 13781–13792.

Rice, R. A., J. Pham, R. J. Lee, A. R. Najafi, B. L. West, and K. N. Green. 2017. "Microglial Repopulation Resolves Inflammation and Promotes Brain Recovery After Injury." *GLIA* 65: 931–944.

Robinson, S. R., E. C. Hampson, M. N. Munro, and D. I. Vaney. 1993. "Unidirectional Coupling of Gap Junctions Between Neuroglia." *Science* 262: 1072–1074.

Rojas, B., B. I. Gallego, A. I. Ramirez, et al. 2014. "Microglia in Mouse Retina Contralateral to Experimental Glaucoma Exhibit Multiple Signs of Activation in all Retinal Layers." *Journal of Neuroinflammation* 11: 133.

Rothhammer, V., D. M. Borucki, E. C. Tjon, et al. 2018. "Microglial Control of Astrocytes in Response to Microbial Metabolites." *Nature* 557, no. 7707: 724–728. https://doi.org/10.1038/s41586-018-0119-x.

Rothhammer, V., and F. J. Quintana. 2019. "The Aryl Hydrocarbon Receptor: An Environmental Sensor Integrating Immune Responses in Health and Disease." *Nature Reviews. Immunology* 19: 184–197.

Saez, J. C., M. A. Retamal, D. Basilio, F. F. Bukauskas, and M. V. Bennett. 2005. "Connexin-Based Gap Junction Hemichannels: Gating Mechanisms." *Biochimica et Biophysica Acta* 1711: 215–224.

Sappington, R. M., B. J. Carlson, S. D. Crish, and D. J. Calkins. 2010. "The Microbead Occlusion Model: A Paradigm for Induced Ocular Hypertension in Rats and Mice." *Investigative Ophthalmology & Visual Science* 51: 207–216.

Saszik, S. M., J. G. Robson, and L. J. Frishman. 2002. "The Scotopic Threshold Response of the Dark-Adapted Electroretinogram of the Mouse." *Journal of Physiology* 543: 899–916.

Sawada, H., T. Fukuchi, T. Tanaka, and H. Abe. 2010. "Tumor Necrosis Factor-Alpha Concentrations in the Aqueous Humor of Patients With Glaucoma." *Investigative Ophthalmology & Visual Science* 51: 903–906.

Schroeter, M., S. Jander, I. Huitinga, O. W. Witte, and G. Stoll. 1997. "Phagocytic Response in Photochemically Induced Infarction of Rat Cerebral Cortex. The Role of Resident Microglia." *Stroke* 28: 382–386.

Slavi, N., A. H. Toychiev, S. Kosmidis, et al. 2018. "Suppression of Connexin 43 Phosphorylation Promotes Astrocyte Survival and Vascular Regeneration in Proliferative Retinopathy." *Proceedings of the National Academy of Sciences of the United States of America* 115: E5934–E5943.

Sofroniew, M. V., and H. V. Vinters. 2010. "Astrocytes: Biology and Pathology." *Acta Neuropathologica* 119: 7–35.

Sterling, J. K., M. O. Adetunji, S. Guttha, et al. 2020. "GLP-1 Receptor Agonist NLY01 Reduces Retinal Inflammation and Neuron Death Secondary to Ocular Hypertension." *Cell Reports* 33: 108271.

Sun, D., and T. C. Jakobs. 2012. "Structural Remodeling of Astrocytes in the Injured CNS." *Neuroscientist: A Review Journal Bringing Neurobiology, Neurology and Psychiatry* 18: 567–588.

Sun, D., S. Moore, and T. C. Jakobs. 2017. "Optic Nerve Astrocyte Reactivity Protects Function in Experimental Glaucoma and Other Nerve Injuries." *Journal of Experimental Medicine* 214: 1411–1430.

Tan, Z., Y. Guo, M. Shrestha, D. Sun, M. Gregory-Ksander, and T. C. Jakobs. 2022. "Microglia Depletion Exacerbates Retinal Ganglion Cell Loss in a Mouse Model of Glaucoma." *Experimental Eye Research* 225: 109273.

Tehrani, S., L. Davis, W. O. Cepurna, et al. 2016. "Astrocyte Structural and Molecular Response to Elevated Intraocular Pressure Occurs Rapidly and Precedes Axonal Tubulin Rearrangement Within the Optic Nerve Head in a Rat Model." *PLoS One* 11: e0167364.

Tehrani, S., E. C. Johnson, W. O. Cepurna, and J. C. Morrison. 2014. "Astrocyte Processes Label for Filamentous Actin and Reorient Early Within the Optic Nerve Head in a Rat Glaucoma Model." *Investigative Ophthalmology & Visual Science* 55: 6945–6952.

Tezel, G. 2008. "TNF-Alpha Signaling in Glaucomatous Neurodegeneration." *Progress in Brain Research* 173: 409–421.

Tezel, G., and Fourth APORICWG. 2009. "The Role of Glia, Mitochondria, and the Immune System in Glaucoma." *Investigative Ophthalmology & Visual Science* 50: 1001–1012.

Toychiev, A. H., K. Batsuuri, and M. Srinivas. 2021. "Gap Junctional Coupling Between Retinal Astrocytes Exacerbates Neuronal Damage in Ischemia-Reperfusion Injury." *Investigative Ophthalmology & Visual Science* 62: 27.

Tribble, J. R., J. M. Harder, P. A. Williams, and S. W. M. John. 2020. "Ocular Hypertension Suppresses Homeostatic Gene Expression in Optic Nerve Head Microglia of DBA/2 J Mice." *Molecular Brain* 13: 81.

Velten, I. M., M. Korth, and F. K. Horn. 2001. "The A-Wave of the Dark Adapted Electroretinogram in Glaucomas: Are Photoreceptors Affected?" *British Journal of Ophthalmology* 85: 397–402.

Wang, J., and Y. Dong. 2016. "Characterization of Intraocular Pressure Pattern and Changes of Retinal Ganglion Cells in DBA2J Glaucoma Mice." *International Journal of Ophthalmology* 9: 211–217.

Wang, N., E. De Vuyst, R. Ponsaerts, et al. 2013. "Selective Inhibition of Cx43 Hemichannels by Gap19 and Its Impact on Myocardial Ischemia/Reperfusion Injury." *Basic Research in Cardiology* 108: 309.

Wheeler, M. A., I. C. Clark, E. C. Tjon, et al. 2020. "MAFG-Driven Astrocytes Promote CNS Inflammation." *Nature* 578, no. 7796: 593–599. https://doi.org/10.1038/s41586-020-1999-0.

Wilson, G. N., D. M. Inman, C. M. Dengler Crish, M. A. Smith, and S. D. Crish. 2015. "Early Pro-Inflammatory Cytokine Elevations in the DBA/2J Mouse Model of Glaucoma." *Journal of Neuroinflammation* 12: 176.

Wohl. 2011. "Optic Nerve Lesion Increases Cell Proliferation and Nestin Expression in the Adult Mouse Eye In Vivo."

Wu, L. J., K. I. Vadakkan, and M. Zhuo. 2007. "ATP-Induced Chemotaxis of Microglial Processes Requires P2Y Receptor-Activated Initiation of Outward Potassium Currents." *GLIA* 55: 810–821.

Yang, X., Q. Zeng, M. Baris, and G. Tezel. 2020. "Transgenic Inhibition of Astroglial NF-kappaB Restrains the Neuroinflammatory and Neurodegenerative Outcomes of Experimental Mouse Glaucoma." *Journal of Neuroinflammation* 17: 252.

Yi, C., P. Ezan, P. Fernández, et al. 2017. "Inhibition of Glial Hemichannels by Boldine Treatment Reduces Neuronal Suffering in a Murine Model of Alzheimer's Disease." 65, no. 1: 1607–1625. https://doi.org/10.1002/glia.23182.

Young, K., and H. Morrison. 2018. "Quantifying Microglia Morphology From Photomicrographs of Immunohistochemistry Prepared Tissue Using ImageJ." *Journal of Visualized Experiments: JoVE* 136: 57648.

Zahs, K. R., and E. A. Newman. 1997. "Asymmetric Gap Junctional Coupling Between Glial Cells in the Rat Retina." *GLIA* 20: 10–22.

Supporting Information

Additional supporting information can be found online in the Supporting Information section.